

12-12-2017 12:00 PM

## Hepcidin-mediated Iron Regulation in P19 Cells is Detectable by MRI

Kobra Alizadeh Pourbouyeh, *The University of Western Ontario*

Supervisor: Goldhawk, Donna E., *The University of Western Ontario*

A thesis submitted in partial fulfillment of the requirements for the Master of Science degree in Medical Biophysics

© Kobra Alizadeh Pourbouyeh 2017

Follow this and additional works at: <https://ir.lib.uwo.ca/etd>



Part of the [Diagnosis Commons](#), and the [Medical Biophysics Commons](#)

---

### Recommended Citation

Alizadeh Pourbouyeh, Kobra, "Hepcidin-mediated Iron Regulation in P19 Cells is Detectable by MRI" (2017). *Electronic Thesis and Dissertation Repository*. 5141.  
<https://ir.lib.uwo.ca/etd/5141>

This Dissertation/Thesis is brought to you for free and open access by Scholarship@Western. It has been accepted for inclusion in Electronic Thesis and Dissertation Repository by an authorized administrator of Scholarship@Western. For more information, please contact [wlsadmin@uwo.ca](mailto:wlsadmin@uwo.ca).

## Abstract

Magnetic resonance imaging (MRI) can be used to track cellular activities in the body using iron-based contrast agents. However, intrinsic cellular iron handling mechanisms may also influence the detection of magnetic resonance (MR) contrast. For instance, inflammation involves downregulation of iron export in macrophages by the hormone hepcidin, due to degradation of the iron export protein, ferroportin (Fpn). We examined the effect of hepcidin on iron regulation and MR transverse relaxation rates in multi-potent P19 cells, which display high iron export activity, similar to macrophages. In response to varying conditions of iron supplementation, our results showed similar Fpn expression in P19 cells as reported for M2 macrophages. Also, hepcidin treatment resulted in Fpn degradation in P19 cells, similar to the reported response of M1 macrophages. The correlation between total cellular iron content and MR transverse relaxation rates was significantly different between hepcidin and non-hepcidin treated P19 cells, providing a tool to non-invasively distinguish different macrophage phenotypes and potentially improve the monitoring of inflammatory cell activities.

## Keywords

Magnetic resonance imaging (MRI), Cell tracking, Inflammation, P19 cells, Iron export, Ferroportin, Hepcidin.

## Acknowledgments

I would first like to thank my supervisor, Dr. Donna Goldhawk, for all her support during my graduate study. Thank you for your trust in me to work in your lab, for all your time and patience, and for teaching me all I needed to conduct my research. Also, thank you for all your kindness to help my husband and I to feel at home when we first came into Canada.

Next, I would like to thank my committee advisors, Dr. Neil Gelman and Dr. James Koropatnick, for their time and support during my research. Also, I am grateful to our collaborators, Dr. Frank Prato and Dr. Terry Thompson, for their great inputs in this study.

I would also like to thank the members of Goldhawk lab who always helped me when I needed it. Thank you for sharing your experiences in the lab with me. Also, thank you for all your assistance during this project. Specifically, I would like to thank Tabitha McGuire, Daisy Sun, Sarah Donnelly, and Tian Tian Hou and Khalid Abdalla. In addition, thanks to John Butler, Heather Biernaski and Lynn Keenlside for their technical assistance during this project.

Last, but not the least, I would like to thank my family. First is a special thanks to my husband, Hazhir Rasouli, who always encouraged me to move forward in my education and career. Thank you for accompanying me on my journey from Iran to Canada to pursue my studies. Also, I am so grateful to my parents who were always there for me. Thank you for all your support and kindness during my life. Also, thank you for believing in me when I decided to follow my dreams in another country. It is all because of you, my family, that I am here right now.

# Table of Contents

Abstract .....	i
Acknowledgments.....	ii
Table of Contents .....	iii
List of Tables .....	vi
List of Figures .....	vii
List of Appendices .....	viii
Chapter 1 .....	1
1 Introduction .....	1
1.1 Importance of Inflammation .....	1
1.2 Molecular Imaging of Inflammation.....	2
1.3 Systemic and Cellular Iron Regulation in Health and Inflammation.....	4
1.4 MRI Relaxometry .....	10
1.5 Overview of the Thesis: .....	15
1.5.1 Hypothesis.....	16
1.5.2 Thesis Objectives .....	16
References.....	18
Chapter 2.....	25
2 Hepcidin-mediated Iron Regulation in P19 Cells is Detectable by MRI .....	25
2.1 Introduction.....	25
2.2 Method .....	26
2.2.1 P19 Cell Culture and Treatment .....	26
2.2.1.1 Cell Model .....	26
2.2.1.2 Iron Supplementation .....	26
2.2.1.3 Hepcidin Treatment .....	27

2.2.2	Protein Expression .....	27
2.2.2.1	Protein Assay .....	27
2.2.2.2	Western Blot .....	28
2.2.3	Trace Element Analysis .....	30
2.2.4	MRI of P19 Cells .....	30
2.2.4.1	Cell Harvest and Phantom Preparation.....	30
2.2.4.2	Data Acquisition and Relaxation Rate Calculation .....	30
2.2.4.3	Region of Interest and Relaxation Rate Measurements .....	31
2.2.5	Statistics .....	32
2.3	Results.....	32
2.3.1	P19 Response to Extracellular Iron Supplementation .....	32
2.3.1.1	Analysis of Intracellular Iron Content .....	32
2.3.1.2	Expression of Ferroportin .....	33
2.3.1.3	MRI Relaxation Rates .....	36
2.3.2	P19 Response to Hepcidin Treatment.....	39
2.3.2.1	Analysis of Intracellular Iron Content .....	39
2.3.2.2	Expression of Ferroportin .....	39
2.3.2.3	MRI Relaxation Rates .....	42
2.3.3	Correlation Between MR Signal and Cellular Iron Content .....	44
2.4	Discussion .....	47
	References .....	54
	Chapter 3 .....	57
3.1	Summary .....	57
3.2	Future Work .....	57
	References .....	60
	Appendix A: P19 response to hepcidin treatment (hepcidin added at 1h-Fe). .....	61

Curriculum Vitae .....	63
------------------------	----

## List of Tables

Table 1. Correlation between MR relaxation rates and total cellular iron content in P19 cells.	
.....	46

## List of Figures

Figure 1.1. Cellular iron homeostasis. ....	5
Figure 1.2. Systemic iron metabolism. ....	6
Figure 1.3. Iron handling in M1 and M2 macrophages. ....	9
Figure 1.4. Spin echo pulse sequence and corresponding FID. ....	13
Figure 1.5. Gradient echo sequence and corresponding FID. ....	14
Figure 2.1. Flow chart of P9 cell sample preparation. ....	28
Figure 2.2. MRI cell phantom and slice localization. ....	31
Figure 2.3. Iron handling in P19 cells under various conditions of extracellular iron supplementation. ....	34
Figure 2.4. Transverse relaxation rate measurement and mapping in the spherical phantom. ....	37
Figure 2.5. Transverse relaxation rates of P19 cells under various conditions of extracellular iron supplementation. ....	38
Figure 2.6. Cellular iron handling in P19 cells in response to hepcidin treatment. ....	40
Figure 2.7. Transverse relaxation rates of P19 cells in response to hepcidin treatment. ....	43
Figure 2.8 Comparison of MR relaxation rates and total cellular iron content in P19 cells...	45



## List of Appendices

Appendix A: P19 response to hepcidin treatment (hepcidin added at 1h-Fe). .....	61
---	----

## Chapter 1

### 1 Introduction

#### 1.1 Importance of Inflammation

Inflammation is the immune system response to noxious stimuli such as pathogen or cell damage. The inflammatory response is activated in a variety of diseases, including cancer and myocardial infarction, to resolve the detrimental stimuli and repair the tissue. This response involves the activation and function of immune system cells such as lymphocytes, for antibody production and cytotoxic enzyme secretion, as well as monocytes and neutrophils, for phagocytosis (1, 2). More specifically, when inflammation is induced, monocytes which are derived from bone marrow stem cells, are recruited to the endangered tissue from the circulation and differentiate into macrophages (3, 4) to help remove detrimental stimuli and facilitate the tissue repair process. The function of these 'activated' macrophages ranges from pro-inflammatory activities, like secretion of pro-inflammatory cytokines to kill microorganisms and damaged cells, to anti-inflammatory activities that facilitate cell debris phagocytosis, inflammation resolution, tissue remodeling and tissue repair (2-4). However, inflammation is not always resolved successfully, resulting in several inflammation associated diseases in humans (1). For instance, chronic inflammation is a condition of sustained pro-inflammatory response which may lead to hypoferremia or tissue damage (1, 2). On the other hand, a prolonged anti-inflammatory phase may lead to unwanted tissue remodeling which impairs tissue function, as seen after myocardial infarction (5-8). In addition, tumor associated macrophages may favor tumor growth by inducing cytokines involved in repair, remodeling and neo-angiogenesis (1, 2, 9). Thus, inflammation is an important process to monitor, whether to achieve an early stage diagnosis of the disease or to assess the tissue response to therapy. Being able to monitor inflammation over time can also improve the outcome of therapy. If the anti-inflammatory therapy is given too early, pathogens may not have been completely cleared. In contrast, if the therapy is given late, unwanted tissue remodeling may result in organ failure. Therefore, developing a tool to

track immune cell activities can improve our understanding of the biology underlying diseases as well as the effectiveness of therapies.

Molecular imaging has emerged as a technique to track cellular and molecular processes involved in various diseases. The ultimate goal in this field is to establish disease-specific imaging biomarkers to enable in vivo monitoring of disease progression as well as its response to therapy. The current status of molecular imaging of inflammation is examined in greater detail.

## 1.2 Molecular Imaging of Inflammation

Various molecular imaging modalities have been examined in pre-clinical and clinical trials to monitor inflammation. Macrophages are attractive tracking targets since they accumulate in large numbers in the inflamed tissue (refer also to section 1.3). In addition, their endocytotic activity is ideal for the uptake of nanoparticles that provide contrast agents for imaging.

Positron emission tomography (PET) is a highly sensitive technique for obtaining functional cellular and molecular information in a variety of diseases (10-12). In this technique, a positron-emitting radioisotope is tagged to a molecule that accumulates in the targeted cell and generates a signal by annihilation with nearby electrons and emission of two photons in opposite directions. Combining PET with magnetic resonance imaging (MRI) or computed tomography (CT), adds anatomical details to the functional information, providing a promising tool for disease monitoring (13-19). Several PET tracers have been developed using  $^{89}\text{Zr}$  (20),  $^{64}\text{Cu}$  (21),  $^{124}\text{I}$  (22) or  $^{18}\text{F}$  (23) for inflammation imaging. The most commonly used PET tracer in the clinic is  $^{18}\text{F}$ -2'-deoxy-2-fluoro-d-glucose ( $^{18}\text{F}$ -FDG), an analog of glucose.  $^{18}\text{F}$ -FDG is taken up by macrophages present in the inflammatory site and provides functional information of the abnormality. However, it also accumulates in the brain and heart. As a result, detecting inflammation foci in those organs will not be specific using this radiotracer (24, 25). In addition,  $^{18}\text{F}$ -FDG is phagocytosed in both pro-inflammatory and anti-inflammatory macrophages (26), making it difficult to distinguish different stages of inflammation.

MRI is a non-invasive imaging modality that utilizes static and varying magnetic fields as well as radiofrequency (RF) waves to obtain superb anatomical detail at any tissue depth (27). The mechanism of signal generation and signal detection in MRI will be discussed in detail in section 1.4. MRI contrast agents were initially developed to improve the detection of anatomical features. Today, however, several MRI contrast agents have been developed to improve the tracking of cellular and molecular activities (25). These contrast agents are divided into two main groups: exogenous agents and endogenous agents. Exogenous agents are chemically synthesized compounds such as superparamagnetic iron oxide nanoparticles (SPIONs) or gadolinium based chelates, which accumulate in the cells of interest (28-30). On the other hand, endogenous agents are reporter genes, overexpressed in the cells of interest to generate MR contrast in a protein-directed process (31-34). In particular, iron biominerals synthesized by magnetotactic bacteria in a membrane-enclosed compartment, termed the magnetosome, are an interesting alternative to chemically synthesized contrast agents. This structure is assembled in a protein-directed process that may be genetically manipulated (35, 36) and provides a model upon which to fashion MRI contrast (33, 34).

Regarding iron-based contrast agents, whether exogenous or endogenous, it is expected that cellular iron-handling activities might affect the accumulation of these agents in the target cells and hence influence MR signal detection (37). As will be described in detail, inflammation-associated cells, *i.e.* macrophages, have distinct iron-handling activity. This may influence the MR detection of inflammatory processes using iron-based agents. It is therefore worth considering the effect of iron handling activity in macrophages, in the context of monitoring inflammation by MRI. What follows is first a description of iron regulation in inflammation compared to the healthy state (1.3) and then a discussion of the mechanism of signal detection in MRI, including the influence of contrast agents (section 1.4). Finally, the potential effect of inflammation-related iron regulation on MRI signal detection will be investigated using a cell model relevant to macrophage activity.

### 1.3 Systemic and Cellular Iron Regulation in Health and Inflammation

#### Cellular iron regulation:

All living organisms require iron for various types of cellular activities such as DNA synthesis and energy metabolism (38). At the cellular level, iron uptake, storage and export is mediated through specific proteins. In vertebrates, non-heme iron in serum is mainly bound to the protein transferrin (Tf) in the form of ferric ion, Fe (III). Tf-bound iron enters the cells through a receptor mediated process involving the transferrin receptor (TfRc). This is followed by reduction of Fe (III) to ferrous iron, Fe (II). The latter species is transported across the endosomal membrane by divalent metal ion transporter 1 (DMT1) and enters the labile iron pool (LIP), a transitory and redox-active source of iron. The majority of imported iron is stored in ferritin, an iron storage protein that oxidizes Fe (II) to Fe (III) as it forms the ferrihydrite (iron oxide) biomineral. While some imported iron is consumed by intracellular activities, the rest is exported from cells by the only known iron export protein in vertebrates, ferroportin (Fpn). Fpn-dependent iron export is also an oxidative process in which Fe (II) in the LIP is released to the extracellular matrix as Fe (III). These key steps complete the loop of cellular iron recycling machinery (**Figure 1.1**) (reviewed in (39)).

Expression of cellular iron regulatory proteins is controlled post-transcriptionally by iron response protein (IRP) and iron response elements (IRE). IRE are hairpin structures found on the 3' end of TfRc mRNA and 5' end of ferritin subunits and Fpn mRNA. Therefore, regulation of Fpn and ferritin in response to iron level are linked. In the case of cellular iron overload, iron binds to IRP, preventing its binding to IRE. This in turn results in downregulation of the transferrin receptor to prevent further iron uptake; upregulation of ferritin to increase iron storage; and in some cells, upregulation of Fpn to export iron. In contrast, low cellular iron leads to upregulation of transferrin receptor and downregulation of ferritin and Fpn (37, 39). The expression of these proteins depends on the cell type and microenvironmental stimuli which will be discussed more in the next section.

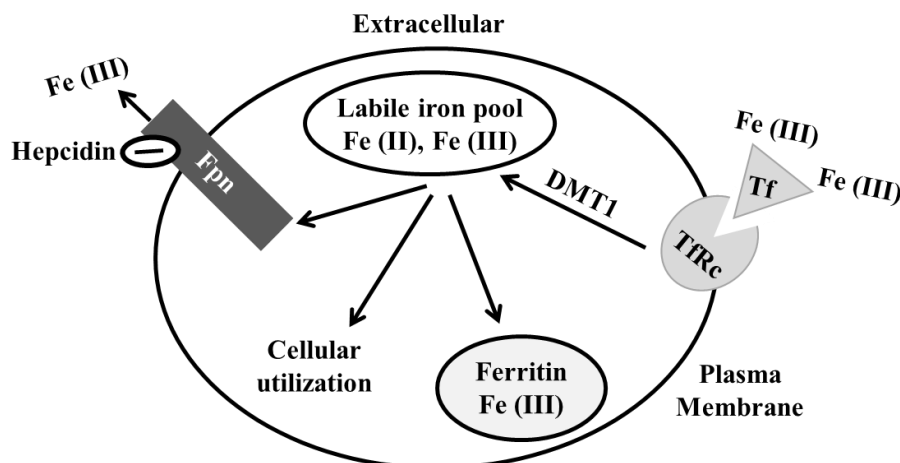


**Figure 1.1. Cellular iron homeostasis.**

Cells take up Tf-bound Fe (III) from plasma through a receptor-mediated interaction (Tf-TfRc). Iron is then reduced and shuttled to a transient, redox-active labile iron pool by DMT1, for use by cellular activities or for storage in ferritin. Fpn returns iron back to the plasma and hepcidin negatively regulates iron export. Tf, transferrin; TfRc, transferrin receptor; Fpn, ferroportin; DMT1, divalent metal ion transporter 1; Fe (II), ferrous iron; Fe (III), ferric iron. The image is modified from Goldhawk *et al*, 2015 (37).

### Systemic iron balance:

Besides various cellular activities, iron is predominantly utilized in erythropoiesis in vertebrates. For instance, erythropoiesis requires about  $2\text{--}3 \times 10^{15}$  iron atoms per second in humans (40). Dietary iron is one source of this element and is mainly absorbed by duodenal enterocytes (41) and stored in liver hepatocytes. However, iron uptake from diet is limited. Thus, vertebrates have evolved to maintain their iron resource through recycling. Macrophages, which are phagocytic cells of the immune system, are responsible for iron recycling in the body. Since red blood cells (RBCs) are the main utilizers of iron, recycling iron from engulfed senescent RBCs by spleen macrophages satisfies the majority of the daily iron requirement (40). In summary, iron is released to plasma from iron recycling macrophages, iron absorbing enterocytes and hepatic storage via the iron export protein, Fpn, which is also known as MTP1, Slc11a3, Slc40a1 and IREG1 (42-44) (Figure 1.2).

Despite the physiological benefits of iron, it also catalyzes the formation of reactive oxygen species (ROS) which may cause tissue damage. Since excess iron is not excreted, systemic iron is tightly regulated at the level of absorption, to provide cells with sufficient iron but prevent iron toxicity. The systemic iron balance is controlled by the regulation of Fpn expression on macrophages, enterocytes and hepatocytes (45). As will be described, Fpn expression is regulated transcriptionally, post-transcriptionally and post-translationally.

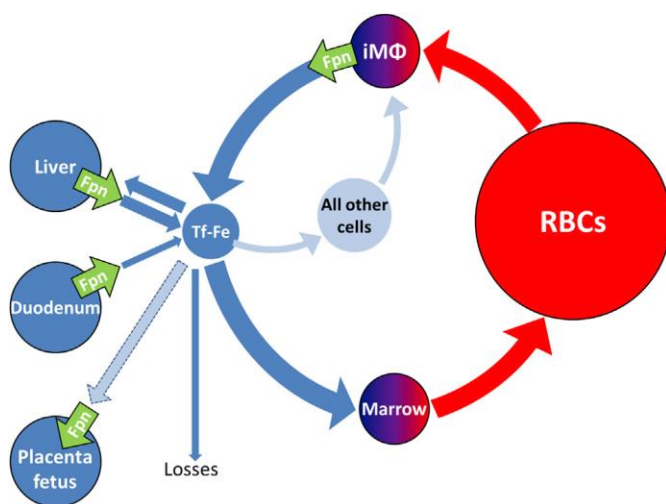


**Figure 1.2. Systemic iron metabolism.**

Dietary iron is absorbed in the duodenum by enterocytes and mainly stored in liver hepatocytes. Ferroportin (Fpn), the only known iron export protein, mediates iron release from these cells into plasma. Transferrin bound iron (Tf-Fe) in serum is then used for red blood cell

production and other cellular activities. Iron from senescent red blood cells and other dead cells is recycled by macrophages (iMΦ) through their Fpn activity. (Image retrieved from (40))

### **Regulation of iron export protein, ferroportin (Fpn):**

At a transcriptional level, hypoxia and anemia upregulate *Fpn* mRNA (40, 46, 47), leading to increased iron release into plasma for erythropoiesis. *Fpn* transcription is also induced by iron accumulation in macrophages after erythrophagocytosis (48-50). On the other hand, *Fpn* transcription is suppressed in splenic macrophages and the intestine during inflammation (51, 52).

*Fpn* expression is also regulated post-transcriptionally in response to cellular iron level. As described earlier, *Fpn* mRNA contains (IRE) at its 5' end which binds cytoplasmic IRP during cellular iron deficiency. This represses *Fpn* translation by sterically

interfering with ribosomal machinery (53). In contrast, increased cellular iron, for instance after erythrophagocytosis in macrophages, results in iron binding to IRP and thus prevents its binding to IRE. This removes the repression of *Fpn* translation (54, 55).

Finally, *Fpn* is also regulated post-translationally by the polypeptide hormone hepcidin, which is predominantly produced by hepatocytes (56). Hepcidin, is the master regulator of iron homeostasis and triggers internalization and degradation of *Fpn* (57, 58). This prevents iron export and lowers the level of serum iron. Production of hepcidin itself depends on various factors as discussed in the following section.

### **Regulation of hepcidin:**

Hepcidin is a hepatic peptide found only in vertebrates in three different forms: hepcidin 20-amino acids (aa), hepcidin 22-aa and hepcidin 25-aa (59). Mature hepcidin is the polypeptide with 25 aa and is exclusively involved in iron regulation. Hepcidin expression is upregulated in response to increased iron concentration in serum via the bone morphogenetic protein-mothers against decapentaplegic homolog (BMP-SMAD) pathway. This prevents further increases in serum iron by blocking iron export from its principle sources: macrophages, hepatocytes and enterocytes (60). In contrast, when erythropoiesis increases, for example due to hypoxia, expression of hepcidin is downregulated so that more serum iron will be available for red blood cell production (61).

Inflammation is another important regulator of hepcidin. Upregulation of hepcidin in response to inflammation is due to host defense mechanisms directed against microbial infections. Since iron is a vital element for cellular activities, it is not surprising that iron availability may also favor bacterial growth in the host. Most bacteria have developed complex mechanisms for iron uptake, such as secreting siderophores as high affinity iron binding molecules (62) or lysis of red blood cells to extract iron from heme (63). On the other hand, the host has also developed mechanisms to ensure bacterial iron deprivation. For instance, serum iron is mainly bound to Tf, which reduces the availability of free iron in the body (39, 64). Another tool involves upregulation of hepcidin expression during inflammation through IL-6 signaling (60). This results in *Fpn* degradation and prevents



iron export from key cells, including macrophages, thus limiting the availability of serum iron for bacterial purposes (51, 65). Since macrophages are key components of both iron recycling and the inflammatory response, the following section examines different macrophage phenotypes and their iron handling roles in the presence and absence of inflammation.

### **Macrophages and iron handling:**

Macrophages are cells of the immune system, originating from blood monocytes which themselves arise from bone marrow stem cells. Macrophages, either circulating in the blood or resident in tissues, have phagocytic functionality to remove cell debris after apoptosis or invasion of bacteria and parasites. Depending on microenvironmental cues, macrophages may polarize into a wide range of phenotypes (3, 66) which dictate their iron handling (67). As described previously, under healthy conditions, iron recycling macrophages show high expression of Fpn which allows them to effectively recycle iron back to the circulation. On the other hand, when pathogen-associated or danger-associated molecular patterns are recognized by host cells, a pro-inflammatory response is induced through release of cytokines and chemokines (2). This invokes monocyte recruitment to the inflamed tissue in a chemokine dependent manner. When these monocytes differentiate to macrophages, they then polarize in a cytokine-dependent manner into pro-inflammatory (classically activated) M1 macrophages (3). M1 macrophages themselves increase production of pro-inflammatory cytokines and have antimicrobial activity. In the context of iron homeostasis, M1 macrophages express Fpn at a minimal level and hence display low iron export activity, but relatively high ferritin expression to retain iron (67). In addition, Fpn protein in M1 macrophages is degraded in response to the increased level of circulating hepcidin, as part of pro-inflammatory signaling. As a result, inflammation is an anti-bacterial response, producing M1 macrophages with an iron retention phenotype to reduce bacterial access to iron. On the other hand, anti-inflammatory (alternatively activated) M2 macrophages are involved in resolution of the inflammation phase, with important roles in tissue repair and wound healing. These M2 cells express higher levels of Fpn and lower levels of ferritin, giving them an iron exporting phenotype (67). The key differences in iron handling activity

between M1 and M2 macrophages are summarized in

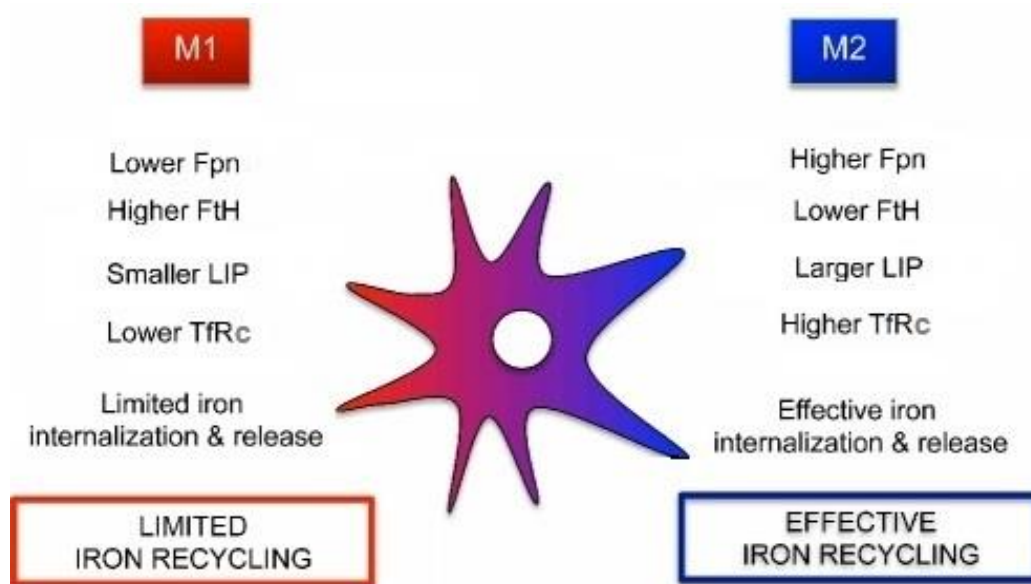


**Figure 1.3.** M2 macrophages engulf cell debris after resolution of inflammation and export cellular iron to replenish the supply in serum. In addition, M2 macrophages activate anti-inflammatory cytokines to stop inflammatory signaling and secrete growth factors to promote tissue repair. It is noteworthy that tumor associated macrophages have similar iron handling properties as M2 macrophages and hence may promote tumor

progression (9, 68). Therefore, macrophages are important components of microbial infection, inflammation and tumorigenesis.

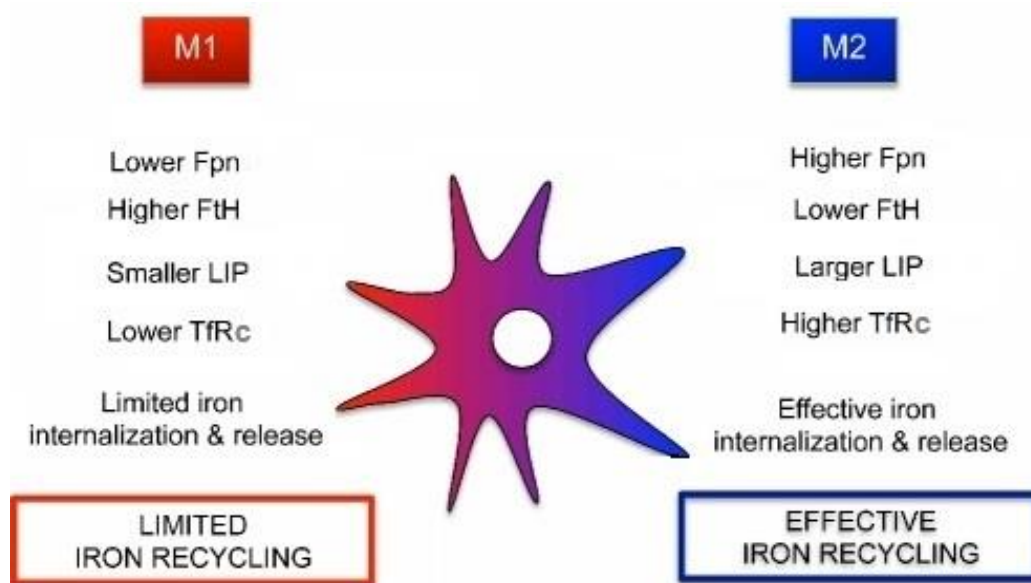


**Figure 1.3. Iron handling in M1 and M2 macrophages.**

M1 macrophages represent an iron-storage phenotype with low Fpn and high FtH expression, while M2 macrophages have iron-recycling properties with high Fpn and low FtH expression. Fpn, ferroportin; FtH, ferritin (heavy chain); LIP, labile iron pool; TfRc, transferrin receptor. The image was retrieved and modified from Corna *et al* (67).

As discussed so far, macrophages have key roles in diseases with inflammatory components and accumulate in high numbers at sites of inflammation. Therefore, macrophages are interesting targets for inflammation monitoring and therapy. In addition, hepcidin dependent downregulation of Fpn in M1 macrophages, in response to inflammation, and their associated iron retention may provide a mechanism to distinguish them from M2 macrophages using molecular imaging. This may give us a better understanding of inflammation progression as well as its response to therapy.

Magnetic resonance imaging (MRI) is a non-invasive imaging modality which has been widely used to monitor macrophages. Various studies have been performed to label and track macrophages using exogenous iron-based MRI contrast agents (69-72). However, the influence of altered macrophage iron homeostasis on the MRI signal, in response to

inflammation, has not been established. In the next section, the basics of MRI signal generation and the influence of iron particles will be described. In chapter 2, we will examine an iron exporting cell type, called P19, to model M2 macrophage activity and investigate if P19 cells may show the phenotypic M1 iron handling in response to hepcidin.

## 1.4 MRI Relaxometry

To understand how iron particles might affect MRI signals, the physics of MRI will be briefly described.

As a general overview of MRI, the subject (patient, animal model or phantom) is surrounded by a magnet and, after excitation by a radiofrequency (RF) pulse, emits signals that will be collected by detectors. This signal is then used in image reconstruction to visualize different organs and tissues (73).

Each atom's nucleus consists of neutral particles called neutrons and positively charged particles called protons. Each proton spins around its axis with a small magnetic moment ( $\mu$ ). Normally, magnetic moment vectors align in random directions, resulting in zero *net* magnetization ( $\underline{M}=0$ ). When the object is placed in an external magnetic field such as the MRI magnet (magnetic field:  $\underline{B}_0$ ), due to the interaction between the external magnetic field and spins, spins start to precess with Larmor frequency ( $\omega_0$ ) which is given by the equation below:

$$\omega_0 = \gamma B_0 \quad [1.1]$$

In equation 1.1,  $B_0$  is the magnitude of the external magnetic field in Tesla (T),  $\omega_0$  is the precession Larmor frequency in radians/sec, and  $\gamma$  is the gyromagnetic ratio. Based on this equation, precession frequency increases proportionally with the strength of the external magnetic field and the exact relationship is determined by  $\gamma$  which has a unique value for each nuclear species. For instance,  $\gamma$  is 42.58 MHz/T for protons ( $H^+$ ), which are the predominant type of atom in the body (73).

Within an external magnetic field, a small fraction of spins aligns parallel to the magnetic field (low energy state), resulting in a non-zero net magnetization. Since this magnetization is parallel to the external magnetic field (and assumed to be in the z direction in a coordinate system), it is called longitudinal magnetization ( $M_z$ ). To obtain a signal, this magnetization needs to be rotated. For this purpose, an oscillating magnetic field ( $B_1$ ), which comes from a RF pulse at the Larmor frequency that is oriented perpendicular to  $B_0$  (i.e., in the x-y plane), is applied to the subject. Because the applied RF pulse has the same frequency as precessing spins, these acquire energy from the pulse which alters their energy state. This phenomenon is called resonance. As a result, some spins will align anti-parallel to the external magnetic field (higher energy states) which results in shortening of the longitudinal magnetization. In addition, magnetic moments will then spin in-phase about the z axis, which results in a newly established transverse magnetization vector in the x-y plane ( $M_{xy}$ ). Due to the  $90^\circ$  change in the direction of magnetization, this RF pulse is also called the  $90^\circ$  pulse.

When the  $90^\circ$  pulse is switched off, the transverse magnetization gradually disappears due to de-phasing of spins after removing the RF pulse. The dephasing process occurs because of the interaction between each spin and its neighbor, resulting in a difference in their precessing frequency that forces them out of phase. This process is called transverse relaxation or spin-spin relaxation and is described by a transverse relaxation time constant,  $T_2$ , which is the time it takes for transverse magnetization to decay to 37% of its original magnitude. In reality, however, inhomogeneities in the local magnetic field may increase the dephasing effect, resulting in a faster dephasing process and shortening the observed transverse relaxation time, denoted as  $T_2^*$  (73). These inhomogeneities are caused by intrinsic defects in the external magnetic field and/or susceptibility-induced field distortions within the tissue.

On the other hand, spins tend to return to their original energy state (also called the equilibrium or relaxation state). Therefore, acquired energy by protons is given to the lattice surrounding them in the form of thermal energy. So, the anti-parallel spins become parallel again, restoring longitudinal magnetization. This process is called longitudinal relaxation or spin-lattice relaxation and is described by a longitudinal relaxation time

constant,  $T_1$ , which is the time it takes for longitudinal magnetization to return to 63% of its original magnitude.

These three relaxation time constants ( $T_1$ ,  $T_2$  and  $T_2^*$ ) can be converted to relaxation rates as follows:  $R_1 = 1/T_1$ ,  $R_2 = 1/T_2$  and  $R_2^* = 1/T_2^*$ . In addition, the difference between  $R_2^*$  (the transverse relaxation rate due to spin-spin interactions and inhomogeneities in an external magnetic field) and  $R_2$  (the irreversible component of transverse relaxation due only to spin-spin interactions) is defined as  $R_2'$ , the reversible component of transverse relaxation due to inhomogeneities in the local magnetic field;  $R_2' = R_2^* - R_2$ .

It is important to mention that transverse magnetization ( $M_{xy}$ ) is constantly precessing with the Larmor frequency as well and therefore, similar to any other oscillating magnetic field, it induces an electrical current in the RF coil elements, which ultimately comprises the MR signal. The magnitude of this signal is proportional to the magnitude of the transverse magnetization ( $M_{xy}$ ) with the same oscillating frequency as  $M_{xy}$ . Since the magnitude of transverse magnetization decreases with time, the signal intensity decreases as well. This signal is called free induction decay (FID).

To be able to measure each relaxation rate, a specific pulse sequence is applied. Each pulse sequence is comprised of RF pulses as well as three gradient magnetic fields which identify the three-dimensional location of the obtained signals. Here we focus on two different types of sequences which will be used in this study; spin echo (SE) and gradient echo (GRE) sequences.

### **Spin echo (SE) Sequence:**

In this sequence, a  $90^\circ$  pulse is applied first to tilt the longitudinal magnetization into the x-y plane, which creates the first FID, followed by one (or multiple)  $180^\circ$  pulses. The purpose of this  $180^\circ$  pulse is to eliminate the de-phasing effect due to inhomogeneities in the local magnetic field by re-phasing the ‘fanning out’ spins and hence increase the magnitude of signal intensity. Time to echo (TE) is the time between the first  $90^\circ$  pulse and when the signal (echo) is refocused. The repetition time (TR) is the time between the two subsequent  $90^\circ$  pulses, where the whole sequence is repeated. The amplitude of the SE signal is described by a decay of the form  $e^{\frac{-t}{T_2}}$ , with a time constant given by  $T_2$  (Figure 1.4).

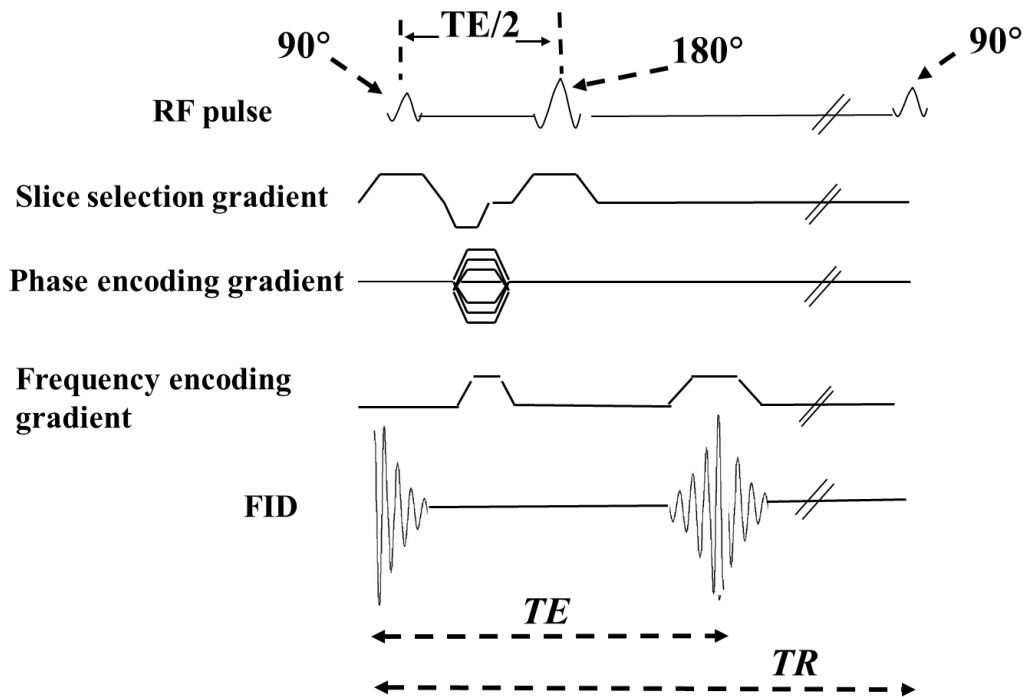


**Figure 1.4. Spin echo pulse sequence and corresponding FID.**

By applying  $180^\circ$  pulses, the effect of inhomogeneities in the local magnetic field is diminished and hence spins that fan out are re-phased. So, the signal decays by  $T_2$ . TE, time to echo; TR, repetition time; FID, free induction decay.

#### **Gradient echo (GRE) sequence:**

In a GRE sequence, signal refocusing is accomplished by a gradient magnetic field which is applied in two opposite directions one after the other, instead of  $180$  pulses. As a result,

the inhomogeneities of the local magnetic field will influence the dephasing of spins and therefore, the decaying curve will be described by  $T_2^*$  instead of  $T_2$ ;  $e^{\frac{-t}{T_2^*}}$  (

**Figure 1.5).**

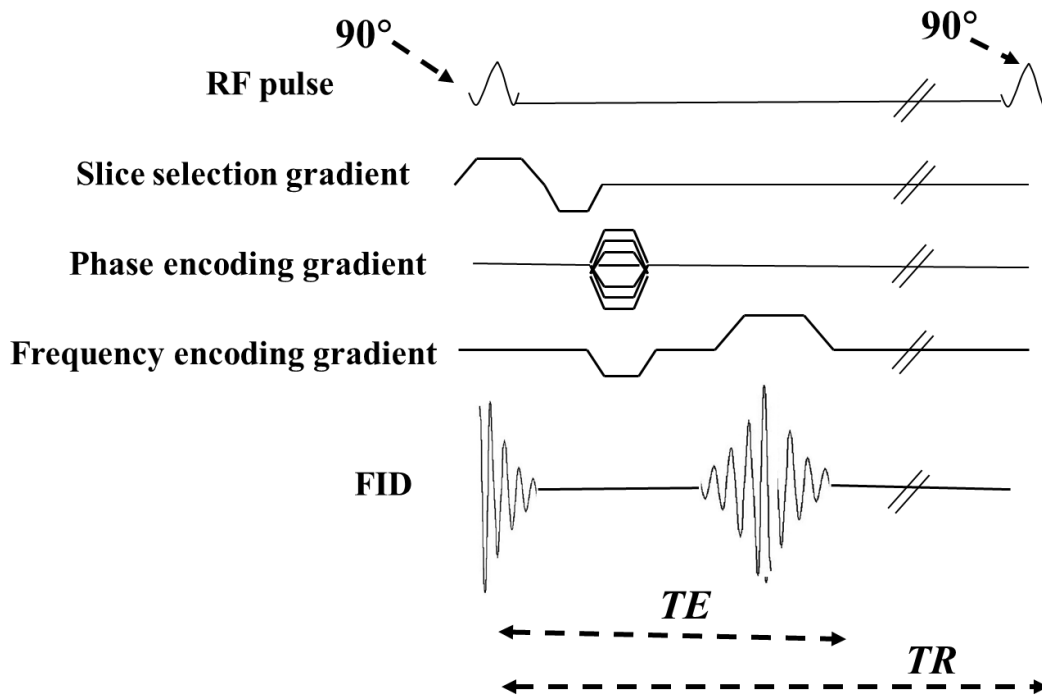


**Figure 1.5. Gradient echo sequence and corresponding FID.**

Since there are no  $180^\circ$  pulses, the signal intensity decays by  $T_2^*$ . TE, time to echo; TR, repetition time; FID, free induction decay.

### **Tissue contrast and contrast agents in MRI:**

Depending on TR and TE, the difference in signal intensity (defined as contrast) between two materials can be explained by their proton density,  $T_1$  and  $T_2$ . With a relatively short TR, for example, the difference in signal intensity between two materials can be distinguished based on their  $T_1$ . This type of image is called  $T_1$ -weighted. By using very long TR, however, the difference explained by  $T_1$  will be diminished. In this case, the difference in signal intensity between two materials can be distinguished based on  $T_2$  if a



long enough TE is chosen. This type of image is called  $T_2$ -weighted. The more  $T_1$  or  $T_2$  relaxation is different between two materials, the more different their signal intensities and therefore the greater the image contrast. This constitutes the basis for using MRI contrast agents. MR contrast agents that result in the shortening of  $T_1$  brighten the MR image in a  $T_1$ -weighted procedure. For this reason, they are called positive contrast agents. Other MR contrast agents result in the shortening of  $T_2$ ; however, this effect results in decreased signal intensity and consequently darkening of the MR image in a  $T_2$ -weighted procedure. As a paramagnetic material, iron shortens the  $T_2$  of atomic nuclei present in the cells in which it has accumulated. Thus, different iron handling activities in different cell types may affect the MR signal. When using iron-based MR contrast agents, it is important to take the iron handling activities of the cell into account. For example, as described earlier, macrophages are immune cells that accumulate at sites of inflammation and display select iron handling activity due to the regulation of Fpn expression by hepcidin. This lead us to investigate the influence of inflammation-related cellular iron regulation on the MRI signal.

## 1.5 Overview of the Thesis:

Inflammation is the immune system's response to cell damage and/or pathogenic threat(s). Macrophages, the main phagocytotic cells of the body, accumulate at the site(s) of injury in response to inflammatory signaling. Macrophages have a distinct role in pathogen removal and tissue repair when polarized to M1 (pro-inflammatory) and M2 (anti-inflammatory) macrophages, respectively, with distinguishable iron handling activity as a result of hepcidin upregulation (66). Hepcidin expression increases in response to inflammation (60) and triggers degradation of the iron export protein, Fpn, present on macrophages. This results in polarization to an M1 phenotype and is part of the host defense mechanism in vertebrates to limit iron availability for bacterial growth. On the other hand, M2 macrophages will actively export iron to facilitate resolution of the inflammatory phase and provide a co-factor required for cell synthesis and tissue repair (3). These features of iron regulation might influence the MRI signal when tracking macrophages and monitoring inflammation. Thus, we investigated the influence of hepcidin-dependent changes in cellular iron regulation on MRI signal detection using

P19 mouse embryonic teratocarcinoma cells as a model of iron export. This multi-potent cell line has shown high iron import and export activity (74), similar to M2 macrophages and can be differentiated into the three germ cell layers: endoderm, mesoderm, and ectoderm. In addition, P19 is a fast-growing cell type, unlike most monocyte or macrophage cell lines, and therefore easy to handle in cell culture.

### 1.5.1 Hypothesis

Downregulation of iron export protein, ferroportin, by hepcidin alters cellular iron content and increases transverse relaxation rates in P19 cells, providing a tractable model of macrophage behavior for molecular imaging of inflammation.

### 1.5.2 Thesis Objectives

The first objective was to examine the expression of Fpn in P19 cells under various conditions of iron supplementation, with or without hepcidin. The regulation of Fpn expression was assessed by Western blot using total protein from P19 cells. We expected that P19 cells would show high Fpn expression when supplemented with extracellular iron, consistent with high iron export activity (74). In addition, we expected Fpn to be degraded in response to hepcidin treatment, consistent with previous reports (57, 58, 75, 76).

The second objective was to investigate the effect of extracellular iron supplementation and hepcidin treatment on cellular iron content in P19 cells. Inductively-coupled plasma mass spectrometry (ICP-MS) analysis was used to determine total cellular iron content in P19 cells. We expected to detect higher cellular iron content in P19 cells supplemented with extracellular iron versus non-supplemented cells. More importantly, for cells treated with hepcidin, higher cellular iron content was expected due to the degradation of iron export protein, Fpn, compared to non-hepcidin treated cells.

The third objective was to determine the influence of different conditions of iron supplementation on the MR transverse relaxation rates in P19 cells. In addition, the influence of hepcidin treatment on MR transverse relaxation rates was examined. When cellular iron increases for cells supplemented with extracellular iron, we expected higher

MR transverse relaxation rates. Also, we expected higher transverse relaxation rates for hepcidin treated cells compared to non-hepcidin treated cells, due to the expected increase in their cellular iron content.

## References

1. Netea M.G., Balkwill F., Chonchol M., Cominelli F., Donath M.Y., Giamarellos-Bourboulis E.J., Golenbock D., Gresnigt M.S., Heneka M.T., Hoffman H.M., Hotchkiss R., Joosten L.A.B., Kastner D.L., Korte M., Latz E., Libby P., Mandrup-Poulsen T., Mantovani A., Mills K.H.G., Nowak K.L., O'Neill L.A., Pickkers P., van der Poll T., Ridker P.M., Schalkwijk J., Schwartz D.A., Siegmund B., Steer C.J., Tilg H., van der Meer J.W.M., van de Veerdonk F.L., Dinarello C.A. *A guiding map for inflammation*. Nat Immunol. [Comment]. 2017;**18**(8):826-31.
2. Ahmed A.U. *An overview of inflammation: mechanism and consequences*. Frontiers in Biology. 2011;**6**:274-81.
3. Gordon S., Taylor P.R. *Monocyte and macrophage heterogeneity*. Nat Rev Immunol. 2005;**5**(12):953-64.
4. Gordon S. *Alternative activation of macrophages*. Nat Rev Immunol. 2003;**3**(1):23-35.
5. Hulsmans M., Sam F., Nahrendorf M. *Monocyte and macrophage contributions to cardiac remodeling*. J Mol Cell Cardiol. 2016;**93**:149-55.
6. Kanellakis P., Ditiatkovski M., Kostolias G., Bobik A. *A pro-fibrotic role for interleukin-4 in cardiac pressure overload*. Cardiovasc Res. 2012;**95**(1):77-85.
7. Sommer M., Eismann U., Gerth J., Stein G. *Interleukin 4 co-stimulates the PDGF-BB- and bFGF-mediated proliferation of mesangial cells and myofibroblasts*. Nephron. 2002;**92**(4):868-80; discussion 80-2.
8. Sempowski G.D., Beckmann M.P., Derdak S., Phipps R.P. *Subsets of murine lung fibroblasts express membrane-bound and soluble IL-4 receptors. Role of IL-4 in enhancing fibroblast proliferation and collagen synthesis*. J Immunol. 1994;**152**(7):3606-14.
9. Komohara Y., Fujiwara Y., Ohnishi K., Takeya M. *Tumor-associated macrophages: Potential therapeutic targets for anti-cancer therapy*. Adv Drug Deliv Rev. 2016;**99**(Pt B):180-5.
10. Gambhir S.S. *Molecular imaging of cancer with positron emission tomography*. Nat Rev Cancer. 2002;**2**(9):683-93.
11. Dobrucki L.W., Sinusas A.J. *PET and SPECT in cardiovascular molecular imaging*. Nat Rev Cardiol. 2010;**7**(1):38-47.
12. Evans N.R., Tarkin J.M., Buscombe J.R., Markus H.S., Rudd J.H.F., Warburton E.A. *PET imaging of the neurovascular interface in cerebrovascular disease*. Nat Rev Neurol. 2017;**13**(11):676-88.

13. Glaudemans A.W.J.M., de Vries E.F.J., Galli F., Dierckx R.A.J.O., Slart R.H.J.A., Signore A. *The Use of F-FDG-PET/CT for Diagnosis and Treatment Monitoring of Inflammatory and Infectious Diseases*. Clinical and Developmental Immunology. 2013;**2013**:14.
14. Lapa C., Reiter T., Li X., Werner R.A., Samnick S., Jahns R., Buck A.K., Ertl G., Bauer W.R. *Imaging of myocardial inflammation with somatostatin receptor based PET/CT — A comparison to cardiac MRI*. International Journal of Cardiology. 2015;**194**(Supplement C):44-9.
15. Farwell M.D., Pryma D.A., Mankoff D.A. *PET/CT imaging in cancer: current applications and future directions*. Cancer. 2014;**120**(22):3433-45.
16. Wada K., Niitsuma T., Yamaki T., Masuda A., Ito H., Kubo H., Hara T., Takenoshita S., Takeishi Y. *Simultaneous cardiac imaging to detect inflammation and scar tissue with 18F-fluorodeoxyglucose PET/MRI in cardiac sarcoidosis*. Journal of Nuclear Cardiology. [journal article]. 2016;**23**(5):1180-2.
17. Wisenberg G., Mikami Y., White J.A., Blackwood K., Tweedie E.J., Thompson T.R., Prato F.S. *Imaging of post-infarction myocardial inflammation with hybrid FDG PET/MR: feasibility and preliminary findings in a canine model*. Journal of Cardiovascular Magnetic Resonance. [journal article]. 2015;**17**(1):Q19.
18. Lindenberg L., Ahlman M., Turkbey B., Mena E., Choyke P. *Evaluation of Prostate Cancer with PET/MRI*. J Nucl Med. 2016;**57**(Suppl 3):111S-6S.
19. Ho A.M., Kalantari B.N. *PET/MRI: A New Frontier in Breast Cancer Imaging*. Breast J. 2016;**22**(3):261-3.
20. Keliher E.J., Yoo J., Nahrendorf M., Lewis J.S., Marinelli B., Newton A., Pittet M.J., Weissleder R. *89Zr-labeled dextran nanoparticles allow in vivo macrophage imaging*. Bioconjug Chem. 2011;**22**(12):2383-9.
21. Zeng D., Lee N.S., Liu Y., Zhou D., Dence C.S., Wooley K.L., Katzenellenbogen J.A., Welch M.J. *64Cu Core-labeled nanoparticles with high specific activity via metal-free click chemistry*. ACS Nano. 2012;**6**(6):5209-19.
22. Seo J.H., Jeon Y.H., Lee Y.J., Yoon G.S., Won D.I., Ha J.H., Jeong S.Y., Lee S.W., Ahn B.C., Lee J. *Trafficking macrophage migration using reporter gene imaging with human sodium iodide symporter in animal models of inflammation*. J Nucl Med. 2010;**51**(10):1637-43.
23. Nahrendorf M., Keliher E., Marinelli B., Leuschner F., Robbins C.S., Gerszten R.E., Pittet M.J., Swirski F.K., Weissleder R. *Detection of Macrophages in Aortic Aneurysms by Nanoparticle Positron Emission Tomography–Computed Tomography*. Arteriosclerosis, Thrombosis, and Vascular Biology. 2011;**31**(4):750-7.

24. Wu C., Li F., Niu G., Chen X. *PET imaging of inflammation biomarkers*. *Theranostics*. 2013;**3**(7):448-66.
25. Weissleder R., Nahrendorf M., Pittet M.J. *Imaging macrophages with nanoparticles*. *Nat Mater*. 2014;**13**(2):125-38.
26. Satomi T., Ogawa M., Mori I., Ishino S., Kubo K., Magata Y., Nishimoto T. *Comparison of contrast agents for atherosclerosis imaging using cultured macrophages: FDG versus ultrasmall superparamagnetic iron oxide*. *J Nucl Med*. 2013;**54**(6):999-1004.
27. Burtea C., Laurent S., Vander Elst L., Muller R.N. *Contrast agents: magnetic resonance*. *Handb Exp Pharmacol*. 2008;**185**:135-65.
28. Serkova N.J. *Nanoparticle-Based Magnetic Resonance Imaging on Tumor-Associated Macrophages and Inflammation*. *Frontiers in Immunology*. 2017;**8**:590.
29. Neuwelt A., Sidhu N., Hu C.A., Mlady G., Eberhardt S.C., Sillerud L.O. *Iron-based superparamagnetic nanoparticle contrast agents for MRI of infection and inflammation*. *AJR Am J Roentgenol*. 2015;**204**(3):W302-13.
30. Huang C.-H., Tsourkas A. *Gd-based macromolecules and nanoparticles as magnetic resonance contrast agents for molecular imaging*. *Current topics in medicinal chemistry*. 2013;**13**(4):411-21.
31. Bar-Shir A., Liang Y., Chan K.W.Y., Gilad A.A., Bulte J.W.M. *Supercharged green fluorescent proteins as bimodal reporter genes for CEST MRI and optical imaging*. *Chemical communications (Cambridge, England)*. 2015;**51**(23):4869-71.
32. Bar-Shir A., Liu G., Greenberg M.M., Bulte J.W.M., Gilad A.A. *Synthesis of a probe for monitoring HSV1-tk reporter gene expression using chemical exchange saturation transfer MRI*. *Nature protocols*. 2013;**8**(12):10.1038/nprot.2013.140.
33. Goldhawk D.E., Rohani R., Sengupta A., Gelman N., Prato F.S. *Using the magnetosome to model effective gene-based contrast for magnetic resonance imaging*. *Wiley Interdiscip Rev Nanomed Nanobiotechnol*. 2012;**4**:378-88.
34. Goldhawk D.E., Gelman N.R., Thompson T., Prato F.S. *Forming Magnetosome-like Nanoparticles in Mammalian Cells for Molecular MRI* In *Design and Applications of Nanoparticles in Biomedical Imaging* (Bulte, J, and Modo, M, Eds). Switzerland: Springer International Publishing; 2017. p. 187-203.
35. Komeili A. *Molecular mechanisms of compartmentalization and biomineralization in magnetotactic bacteria*. *FEMS microbiology reviews*. 2012;**36**:232-55.
36. Uebe R., Schuler D. *Magnetosome biogenesis in magnetotactic bacteria*. *Nat Rev Microbiol*. 2016;**14**(10):621-37.

37. Goldhawk D.E., Gelman N., Sengupta A., Prato F.S. *The interface between iron metabolism and gene-based iron contrast for MRI*. Magnetic Resonance Insights. 2015;**8**:9-14.
38. Ganz T. *Systemic Iron Homeostasis*. Physiological Reviews. 2013;**93**(4):1721-41.
39. Lane D.J.R., Merlot A.M., Huang M.L.H., Bae D.H., Jansson P.J., Sahni S., Kalinowski D.S., Richardson D.R. *Cellular iron uptake, trafficking and metabolism: Key molecules and mechanisms and their roles in disease*. Biochimica et Biophysica Acta (BBA) - Molecular Cell Research. 2015;**1853**(5):1130-44.
40. Drakesmith H., Nemeth E., Ganz T. *Ironing out Ferroportin*. Cell Metabolism. 2015;**22**(5):777-87.
41. Mackenzie B., Garrick M.D. *Iron Imports. II. Iron uptake at the apical membrane in the intestine*. American Journal of Physiology - Gastrointestinal and Liver Physiology. 2005;**289**(6):G981-G6.
42. Donovan A., Brownlie A., Zhou Y., Shepard J., Pratt S.J., Moynihan J., Paw B.H., Drejer A., Barut B., Zapata A., Law T.C., Brugnara C., Lux S.E., Pinkus G.S., Pinkus J.L., Kingsley P.D., Palis J., Fleming M.D., Andrews N.C., Zon L.I. *Positional cloning of zebrafish ferroportin1 identifies a conserved vertebrate iron exporter*. Nature. 2000;**403**(6771):776-81.
43. Abboud S., Haile D.J. *A novel mammalian iron-regulated protein involved in intracellular iron metabolism*. J Biol Chem. 2000;**275**(26):19906-12.
44. McKie A.T., Marciani P., Rolfs A., Brennan K., Wehr K., Barrow D., Miret S., Bomford A., Peters T.J., Farzaneh F., Hediger M.A., Hentze M.W., Simpson R.J. *A novel duodenal iron-regulated transporter, IREG1, implicated in the basolateral transfer of iron to the circulation*. Mol Cell. 2000;**5**(2):299-309.
45. De Domenico I., McVey Ward D., Kaplan J. *Regulation of iron acquisition and storage: consequences for iron-linked disorders*. Nat Rev Mol Cell Biol. 2008;**9**(1):72-81.
46. Ward D.M., Kaplan J. *Ferroportin-mediated iron transport: expression and regulation*. Biochim Biophys Acta. 2012;**1823**(9):1426-33.
47. Taylor M., Qu A., Anderson E.R., Matsubara T., Martin A., Gonzalez F.J., Shah Y.M. *Hypoxia-inducible factor-2alpha mediates the adaptive increase of intestinal ferroportin during iron deficiency in mice*. Gastroenterology. 2011;**140**(7):2044-55.
48. Knutson M.D., Vafa M.R., Haile D.J., Wessling-Resnick M. *Iron loading and erythrophagocytosis increase ferroportin 1 (FPN1) expression in J774 macrophages*. Blood. 2003;**102**(12):4191-7.

49. Marro S., Chiabrando D., Messana E., Stolte J., Turco E., Tolosano E., Muckenthaler M.U. *Heme controls ferroportin1 (FPN1) transcription involving Bach1, Nrf2 and a MARE/ARE sequence motif at position -7007 of the FPN1 promoter.* Haematologica. 2010;**95**(8):1261-8.
50. Delaby C., Pilard N., Puy H., Canonne-Hergaux F. *Sequential regulation of ferroportin expression after erythrophagocytosis in murine macrophages: early mRNA induction by haem, followed by iron-dependent protein expression.* Biochem J. 2008;**411**(1):123-31.
51. Yang F., Liu X.B., Quinones M., Melby P.C., Ghio A., Haile D.J. *Regulation of reticuloendothelial iron transporter MTP1 (Slc11a3) by inflammation.* J Biol Chem. 2002;**277**(42):39786-91.
52. Liu X.B., Nguyen N.B., Marquess K.D., Yang F., Haile D.J. *Regulation of hepcidin and ferroportin expression by lipopolysaccharide in splenic macrophages.* Blood Cells Mol Dis. 2005;**35**(1):47-56.
53. Lymboussaki A., Pignatti E., Montosi G., Garuti C., Haile D.J., Pietrangelo A. *The role of the iron responsive element in the control of ferroportin1/IREG1/MTP1 gene expression.* J Hepatol. 2003;**39**(5):710-5.
54. Delaby C., Pilard N., Puy H., Canonne-Hergaux F. *Sequential regulation of ferroportin expression after erythrophagocytosis in murine macrophages: early mRNA induction by haem, followed by iron-dependent protein expression.* Biochemical Journal. 2008;**411**(1):123-31.
55. Sangokoya C., Doss J.F., Chi J.T. *Iron-responsive miR-485-3p regulates cellular iron homeostasis by targeting ferroportin.* PLoS Genet. 2013;**9**(4):e1003408.
56. Park C.H., Valore E.V., Waring A.J., Ganz T. *Hepcidin, a urinary antimicrobial peptide synthesized in the liver.* J Biol Chem. 2001;**276**(11):7806-10.
57. Nemeth E., Tuttle M.S., Powelson J., Vaughn M.B., Donovan A., Ward D.M., Ganz T., Kaplan J. *Hepcidin regulates cellular iron efflux by binding to ferroportin and inducing its internalization.* Science (New York, NY). 2004;**306**:2090-3.
58. De Domenico I., Ward D.M., Langelier C., Vaughn M.B., Nemeth E., Sundquist W.I., Ganz T., Musci G., Kaplan J. *The molecular mechanism of hepcidin-mediated ferroportin down-regulation.* Molecular Biology of the Cell. 2007;**18**:2569-78.
59. Kemna E.H.J.M., Tjalsma H., Podust V.N., Swinkels D.W. *Mass Spectrometry-Based Hepcidin Measurements in Serum and Urine: Analytical Aspects and Clinical Implications.* Clinical Chemistry. 2007;**53**(4):620-8.
60. Sangkhae V., Nemeth E. *Regulation of the Iron Homeostatic Hormone Hepcidin.* Adv Nutr. 2017;**8**(1):126-36.



61. Camaschella C., Pagani A. *Iron and erythropoiesis: a dual relationship*. Int J Hematol. 2011;**93**(1):21-6.
62. Schaible U.E., Kaufmann S.H. *Iron and microbial infection*. Nat Rev Microbiol. 2004;**2**(12):946-53.
63. Skaar E.P., Humayun M., Bae T., DeBord K.L., Schneewind O. *Iron-source preference of Staphylococcus aureus infections*. Science (New York, NY). 2004;**305**(5690):1626-8.
64. Recalcati S., Locati M., Cairo G. *Systemic and cellular consequences of macrophage control of iron metabolism*. Semin Immunol. 2012;**24**(6):393-8.
65. Peyssonnaud C., Zinkernagel A.S., Datta V., Lauth X., Johnson R.S., Nizet V. *TLR4-dependent hepcidin expression by myeloid cells in response to bacterial pathogens*. Blood. 2006;**107**(9):3727-32.
66. Martinez F.O., Helming L., Gordon S. *Alternative activation of macrophages: an immunologic functional perspective*. Annu Rev Immunol. 2009;**27**:451-83.
67. Corna G., Campana L., Pignatti E., Castiglioni A., Tagliafico E., Bosurgi L., Campanella A., Brunelli S., Manfredi A.A., Apostoli P., Silvestri L., Camaschella C., Rovere-Querini P. *Polarization dictates iron handling by inflammatory and alternatively activated macrophages*. Haematologica. 2010;**95**:1814-22.
68. Sica A., Schioppa T., Mantovani A., Allavena P. *Tumour-associated macrophages are a distinct M2 polarised population promoting tumour progression: potential targets of anti-cancer therapy*. Eur J Cancer. 2006;**42**(6):717-27.
69. Daldrup-Link H.E., Golovko D., Ruffell B., Denardo D.G., Castaneda R., Ansari C., Rao J., Tikhomirov G.A., Wendland M.F., Corot C., Coussens L.M. *MRI of tumor-associated macrophages with clinically applicable iron oxide nanoparticles*. Clin Cancer Res. 2011;**17**(17):5695-704.
70. Hingorani D.V., Bernstein A.S., Pagel M.D. *A review of responsive MRI contrast agents: 2005–2014*. Contrast media & molecular imaging. 2015;**10**(4):245-65.
71. Chan J.M.S., Cheung M.S.H., Gibbs R.G.J., Bhakoo K.K. *MRI detection of endothelial cell inflammation using targeted superparamagnetic particles of iron oxide (SPIO)*. Clinical and Translational Medicine. 2017;**6**:1.
72. Yilmaz A. *Visualising inflammation after myocardial infarction with the use of iron oxide nanoparticles*. Heart. 2017.
73. Hashemi R.H., Bradley W.G., Lisanti C.J. MRI: The Basics, 2nd Edition: Lippincott Williams & Wilkins; 2004.

74. Liu L. Characterization of MagA expression and Iron uptake in P19 cells: Implications for use as a gene-based contrast agent for MRI: Western Univeristy; 2015.
75. Delaby C., Pilard N., Gonçalves A.S., Beaumont C., Canonne-Hergaux F. *Presence of the iron exporter ferroportin at the plasma membrane of macrophages is enhanced by iron loading and down-regulated by hepcidin.* Blood. 2005;**106**(12):3979-84.
76. Qiao B., Sugianto P., Fung E., del-Castillo-Rueda A., Moran-Jimenez M.-J., Ganz T., Nemeth E. *Hepcidin-induced endocytosis of ferroportin is dependent on ferroportin ubiquitination.* Cell Metabolism. 2012;**15**(6):918-24.

## Chapter 2

# 2 Hepcidin-mediated Iron Regulation in P19 Cells is Detectable by MRI

## 2.1 Introduction

Inflammation is the immune system response to harmful stimuli. This process involves the activation of immune system cells that remove the noxious stimuli and initiate tissue repair (1). In particular, monocytes and macrophages are recruited to the endangered site from the circulation and differentiate into pro-inflammatory (M1) macrophages and anti-inflammatory (M2) macrophages (2). M1 (also called classically activated) macrophages have a distinct role in secreting pro-inflammatory cytokines which facilitate pathogen or damaged cell removal. M2 (also called alternatively activated) macrophages are responsible for inflammation resolution and tissue repair (3).

Interestingly, iron handling mechanisms in these two phenotypes are different. M1 macrophages show low iron export and high iron storage activities by expressing a low level of Fpn, the only recognized iron export protein in vertebrates (4), and a high level of ferritin, respectively (5). In the pathogen removal phase, this represents a host defense mechanism to limit free iron availability for bacterial growth. This occurs in response to upregulation of the endocrine hormone hepcidin during inflammation (6). Hepcidin activity downregulates Fpn, resulting in iron retention in M1 macrophages (7, 8). On the other hand, M2 macrophages show high iron export and low iron storage activities by expressing a high level of Fpn and low level of ferritin, respectively (5). This feature facilitates the tissue repair process by providing iron to adjacent cells as a growth co-factor in the inflammation resolution phase. Being able to distinguish between M1 and M2 macrophages may lead to a better understanding of the different phases of inflammation and improve diagnosis and treatment outcomes.

MRI is a non-invasive imaging method that can be used to track cellular activities involved in different diseases. Toward achieving molecular imaging capability, various iron-based exogenous and endogenous contrast agents have been developed to enhance image contrast (9, 10). Hence, it might be expected that cellular iron handling activities may influence the

accumulation of contrast agents and their detection by MRI (11). In the case of iron exporting cells, particularly pro- and anti-inflammatory macrophages, their distinct iron regulation might even be distinguishable by MRI. To investigate this hypothesis, we used the multi-potent P19 stem cell model, which exhibits high iron import and export activities (12), the latter of which corresponds with high expression of Fpn (11). In this regard, P19 cells resemble macrophages (5) and may provide a convenient model of iron regulation during inflammation. In this study, we examined the effect of varying extracellular iron supplementation and hepcidin signaling on MR contrast in undifferentiated P19 cells, to model the non-invasive detection of molecular activity present during inflammation. Changes in total cellular iron content as well as Fpn expression confirm the influence of iron handling activities on MRI and establish the potential of P19 cells to model inflammatory responses.

## 2.2 Method

### 2.2.1 P19 Cell Culture and Treatment

#### 2.2.1.1 Cell Model

Mouse multipotent teratocarcinoma cells (P19, ATCC<sup>®</sup> CRL-1825<sup>™</sup>) were cultured in alpha-minimum essential medium ( $\alpha$ -MEM). Medium was supplemented with 10% fetal bovine serum (FBS), 4 U/mL penicillin and 4  $\mu$ g/mL streptomycin. Cells were incubated in a humid chamber at 37°C with a 5% CO<sub>2</sub>/air mixture and passaged 1:10 or 1:20 when they reached 70% confluency. Cells were harvested by trituration alone for protein expression analysis or after 30 sec incubation with 0.05% Trypsin/EDTA for trace element analysis and MR relaxation rate measurements. All cell culture reagents were purchased from Life Technologies, Burlington, Canada.

#### 2.2.1.2 Iron Supplementation

A flow chart depicting sample preparation is shown in Figure 2.1. To study the P19 cell response to extracellular iron, cells cultured in standard (non-supplemented) medium (-Fe), were placed in iron-supplemented medium containing 25  $\mu$ M of ferric nitrate (Sigma-Aldrich, Oakville, Canada) for 5-7 days (+Fe). After iron supplementation,

extracellular iron was removed and replaced with non-supplemented medium for an additional 1 (1h-Fe), 2, (2h-Fe), 4 (4h-Fe) and 24 (24h-Fe) hours, to examine iron export activity in P19 cells over time (Figure 2.1, first row). Changes in total cellular iron content, Fpn expression and MR signal were then explored over the treatment timeframe, as will be described.

### 2.2.1.3 Hepcidin Treatment

To investigate the effect of hepcidin, cells were cultured in medium containing 200 ng/mL hepcidin (Sigma-Aldrich, Oakville, Canada) using two different treatments: hepcidin was added either one hour after the removal of extracellular iron supplement (at 1h-Fe; Figure 2.1, second row) or immediately after iron supplement removal (Figure 2.1, third row). These time points for the addition of hepcidin are related to the rate of iron export rate in P19 cells. Based on a previous study, P19 cellular iron content decreased substantially within the first hour following withdrawal of iron supplementation (12). By adding hepcidin at time points in which active iron export was expected, we aimed to block iron export in P19 cells.

In addition, cell samples +/-Fe were incubated with hepcidin for the last 24 hours of culture. This was performed to separate potential changes in the P19 cell response to inflammation (*i.e.* hepcidin) from those changes arising from the combination of hepcidin and increased extracellular iron.

## 2.2.2 Protein Expression

### 2.2.2.1 Protein Assay

Cells were cultured under different conditions of iron supplementation and hepcidin treatment as described above (Figure 2.1). Then, they were washed twice using 10 mL phosphate buffered saline (PBS, 137mM NaCl/2.7 mM KCl/10mM  $\text{HPO}_4^{2-}$ ), collected in 1 mL radioimmunoprecipitation assay buffer (RIPA; 10 mM Tris-HCl pH 7.5/140 mM NaCl/1% NP-40/1% sodium deoxycholate/0.1% sodium dodecyl sulfate [SDS]) containing 150  $\mu\text{L}$  Complete Mini protease inhibitor cocktail (Roche Diagnostic Systems,

Laval, Canada) and lysed by sonication. Total amount of protein was quantified using the BCA protein assay (13).

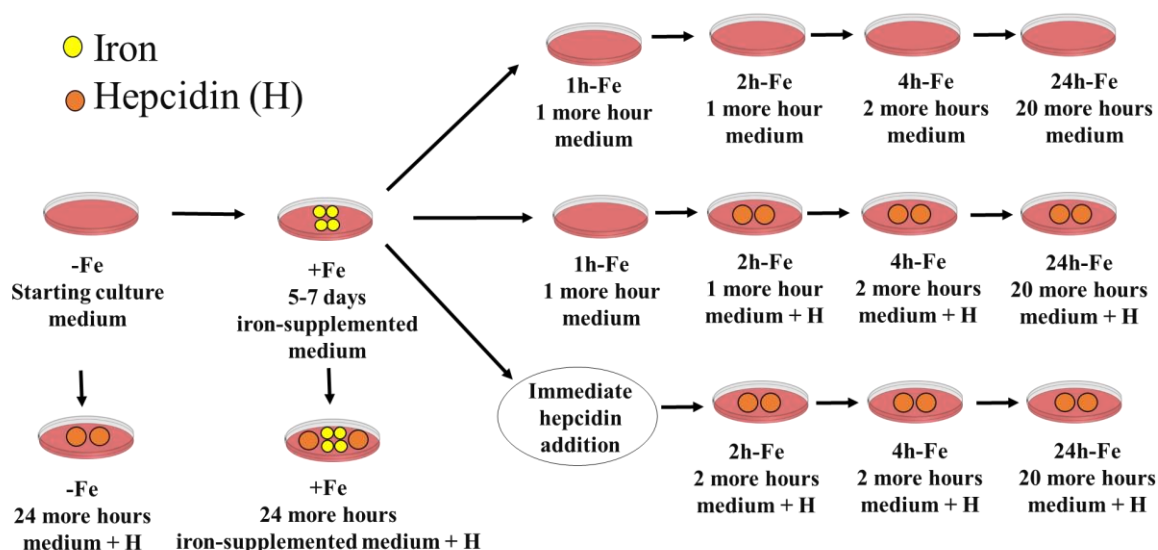


**Figure 2.1. Flow chart of P9 cell sample preparation.**

Cells were cultured in non-supplemented (-Fe) or iron-supplemented (+Fe) medium containing 25  $\mu$ M ferric nitrate for 5-7 days prior to withdrawal of iron supplementation and further culture in non-supplemented medium for an additional 1 (1h-Fe), 2 (2h-Fe), 4 (4h-Fe) or 24 (24h-Fe) hours (first row). To examine the cells' response to hepcidin, 200 ng/ml hepcidin/medium was added to the culture at either 1h-Fe (second row) or immediately after removal of iron supplementation (third row). In addition, -Fe and +Fe samples were incubated with hepcidin for the last 24 hours of culture in non-supplemented (-Fe +H) or iron-supplemented (+Fe +H) medium, respectively. At each time point, live cells were harvested and either prepared for MRI or lysed and analyzed by Western blot (for protein) and inductively-coupled plasma mass spectrometry (ICP-MS, for elemental iron).

### 2.2.2.2 Western Blot

Each Western blot sample was prepared in 30  $\mu$ L total volume containing 20  $\mu$ g of total cellular protein (14). Molecular weight standards were purchased from Thermo Fisher Scientific, Mississauga, Canada. To reduce protein disulfide bonds, 1 mM dithiothreitol (DTT, Thermo Fisher Scientific, Mississauga, Canada) was added to the sample

preparation buffer and samples were heated at 80 °C for 5 minutes prior to electrophoresis. Proteins were separated by sodium dodecyl sulfate polyacrylamide gel electrophoresis (SDS-PAGE) using a 10 % acrylamide running gel and a 5 % acrylamide stacking gel. Proteins were transferred onto nitrocellulose blots (Thermo Fisher Scientific, Mississauga, Canada) using the Original iBlot® Gel Transfer Device (Life Technologies, Burlington, Canada). Nonspecific protein binding was blocked by incubating blots in 5% bovine serum albumin (BSA)/Tris-buffered saline (TBS)/0.02 % sodium azide (TBSA) for a minimum of 2 hours at room temperature. For Fpn detection, blots were incubated with a 1:1000 dilution of rabbit anti-ferroportin 1 antibody (Thermo Fisher Scientific, Mississauga, Canada)/5% BSA/TBSA at 4°C overnight. Then blots were washed using Tris-buffered saline/ 0.1% Tween 20 (TBST), Sigma-Aldrich, Oakville, Canada) for 30 minutes with 4 changes of buffer and incubated for another 1 hour with a 1: 20,000 dilution of horseradish peroxidase (HRP)-conjugated goat anti-rabbit IgG secondary antibody (Sigma-Aldrich, Oakville, Canada)/5% BSA/TBS at room temperature. Finally, blots were washed with 0.1% TBST for another 30 minutes with 2 changes of buffer and were then imaged using the Chemigenius Gel Doc (Syngene). A chemiluminescent signal was detected using SuperSignal West Pico Chemiluminescent Substrate (Thermo Fisher Scientific, Mississauga, Canada) according to the manufacturer's instructions. The reported molecular weight (M.W.) for Fpn is approximately 63 kDa (15, 16).

Glyceraldehyde 3-phosphate dehydrogenase (GAPDH) was used as a control to confirm uniform protein loading in all lanes. For GAPDH detection, blots were probed as detailed above, with the following changes. Blots were incubated overnight in a 1:2000 dilution of rabbit anti-GAPDH antibody (Thermo Fisher Scientific, Mississauga, Canada) and for 1 hour in a 1: 20,000 dilution of HRP-conjugated goat anti-rabbit IgG secondary antibody, all at room temperature. The reported molecular weight for GAPDH is approximately 37 kDa (17).

To assess changes in Fpn expression, the signal intensity of each 63kDa Fpn band was normalized to the corresponding GAPDH band for that sample, using Image Lab

software version 5.2. The results were then normalized to the +Fe (no hepcidin) condition.

### 2.2.3 Trace Element Analysis

At harvest, P19 cells were lysed and protein concentration was determined as described in 2.2.2.1 section. Samples with concentrations of 0.5- 2 mg protein/mL were prepared for trace element analysis. The concentration of elemental iron (Fe) was measured by ICP-MS (Biotron Analytical Services, Western University) and normalized to protein concentration.

### 2.2.4 MRI of P19 Cells

#### 2.2.4.1 Cell Harvest and Phantom Preparation

P19 cells were cultured in four or five 150 mm cell culture dishes to have a sufficient number of cells for this experiment (approximately 40-50 million cells). After harvesting, cells were centrifuged at  $400\times g$  and  $15^{\circ}\text{C}$  for 5 minutes, repeating as needed to obtain the desired compact cell pellet in custom made Ultem wells (Inner diameter: 4 mm and height: 10 mm, Lawson Imaging Prototype Lab). Afterwards, wells were placed in a 9 cm, spherical 4% gelatin (porcine type 1, Sigma-Aldrich, Oakville, Canada)/PBS phantom (18) and overlaid with sterile filtered 4% gelatin/PBS (Figure 2.2a).

#### 2.2.4.2 Data Acquisition and Relaxation Rate Calculation

Using a knee RF coil, the gelatin phantom was scanned on a 3T mMR Biograph (Siemens AG, Erlangen, Germany), using previously described sequences (18), to obtain transverse relaxation rates. Single echo spin echo and multi-echo gradient echo sequences were applied to obtain  $R_2$  and  $R_2^*$ , respectively. The reversible component,  $R_2'$  was calculated by subtraction ( $R_2^* - R_2$ ).



The following imaging parameters were employed. For the single echo spin echo sequence: TE= 13, 30, 40, 60, 80, 100, 150, 200, 300 ms; TR= 2010 ms; flip angle= 90°; total scanning time= approximately 61 minutes. For the multi echo gradient echo sequence: TE= 6.12, 14.64, 23.16, 31.68, 40.2, 50, 60, 70, 79.9 ms; TR= 200 ms; flip angle= 60°; total scanning time= approximately 25 minutes. In both sequences, the field of view was 120×120 mm, the voxel size was 1.5×0.6×0.6 mm<sup>3</sup> and the matrix size was 192×192. The slice thickness was 3 mm, perpendicular to the wells as shown in Figure 2.2b.

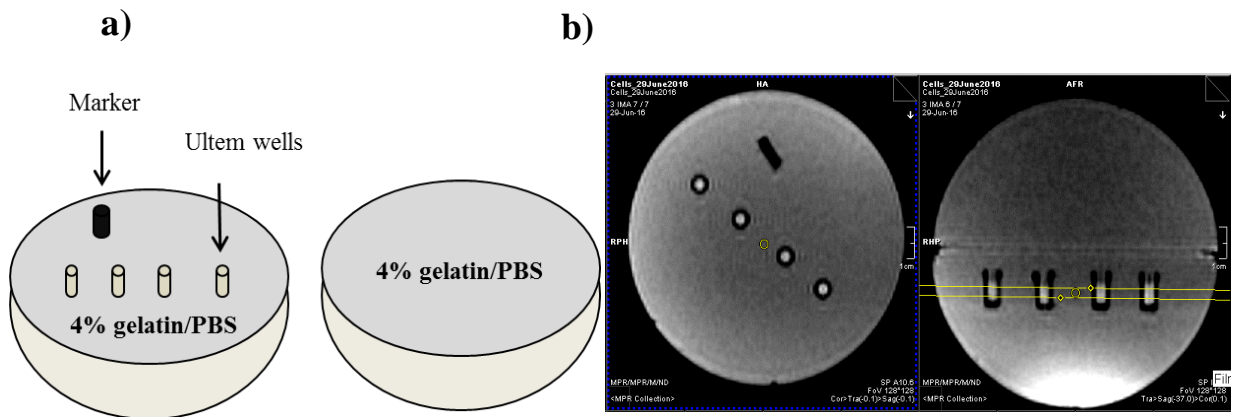


**Figure 2.2. MRI cell phantom and slice localization.**

Two hemispheres of a plastic mold were filled with 4% gelatin/PBS. Cells were placed in Ultem wells in one hemisphere, overlaid with 4% gelatin/PBS and covered by the other hemisphere. Sample orientation was indicated by a plastic peg. b) Using a knee RF coil, images were acquired at 3T. In the cross-sectional view (left panel), the arrangement of sample wells is shown. A 3-mm thick slice was defined for image acquisition by the yellow box in the sagittal view (right panel), perpendicular to the wells.

#### 2.2.4.3 Region of Interest and Relaxation Rate Measurements

Analysis software developed in Matlab 7.9.0 (R2010b) was used to determine region of interest (ROI) and to measure  $R_2^*$  and  $R_2$ . ROI was outlined to include as many voxels as possible within the sample wells while avoiding the wall of the wells. Approximately 21 voxels were included in the circular ROI. Relaxation rates were determined using the average signal intensity for each time point and least-squares curve fitting.

## 2.2.5 Statistics

Mean and standard error of the mean (SEM) were calculated. Two-way analysis of variance (ANOVA) was performed to examine any significant differences among treatment groups ( $p < 0.05$ ). Pearson's correlation was applied to examine potential correlation between cellular iron and relaxation rates and the regression model identifies the best linear equation between each relaxation rate as dependent variable and cellular iron content as independent variable. To compare the slopes of linear correlations, student's t-test was conducted and finally the strength of the correlations was compared using Fisher Z transformation. All statistical analyses were performed using IBM SPSS Statistics, version 25. All graphs were created using the GraphPad Prism package, version 7.03.

## 2.3 Results

### 2.3.1 P19 Response to Extracellular Iron Supplementation

#### 2.3.1.1 Analysis of Intracellular Iron Content

Iron import and export activities in P19 cells were investigated using various conditions of iron supplementation. To examine iron import activity, the cells were cultured in the absence (-Fe) or presence (+Fe) of extracellular iron supplementation (25  $\mu$ M ferric nitrate) for 5-7 days. Regarding iron export activity in P19 cells, initial results from Liu (12) suggested that total cellular iron content decreases within one hour after iron supplementation withdrawal and is reduced to baseline levels after 24 hours. To study iron handling in P19 cells more thoroughly, iron-supplemented cells were harvested either immediately or after additional culture in non-supplemented medium for 1, 2, 4 or 24 hours (Figure 2.1, first row).

Each sample was analyzed by ICP-MS to determine total intracellular iron content. Figure 2.3a) shows the mean values of total cellular iron, normalized to amount of protein. Based on trace element analysis, cellular iron content significantly increased after iron supplementation (+Fe) compared to samples cultured in non-supplemented medium (-Fe) ( $p < 0.05$ ), confirming high iron import activity in P19 cells. However, upon

removal of iron supplementation and continued culture in non-supplemented medium, cellular iron content decreased, reaching baseline values after 4 hours (+Fe versus 4h-Fe,  $p < 0.01$ ), suggesting high iron export activity. Interestingly, cellular iron level increased again, 24 hours after removal of iron supplement (24h-Fe versus 4h-Fe,  $p < 0.05$ ), raising the possibility that P19 cells regulate iron in a biphasic manner. While a typical rise in total cellular iron content was observed one hour after removal of extracellular iron supplement, the difference between +Fe and 1h-Fe was not statistically significant

### 2.3.1.2 Expression of Ferroportin

Possible changes in Fpn protein expression in response to extracellular iron supplementation were examined by Western blot (Figure 2.3b). Prior to electrophoresis, cells were cultured in the presence or absence of extracellular iron supplementation as shown in Figure 2.1, first row. The reported molecular weight (M.W.) for Fpn is approximately 63 kDa (15, 16). The relatively constant expression of GAPDH (M.W. 37 kDa, (17)) gave a uniform band in each lane, as determined by densitometry (data not shown). The ratio of Fpn/GAPDH is shown in Figure 2.3c).

As shown in Figure 2.3b) and c), minimal Fpn expression was detected for cells cultured in non-supplemented medium (-Fe). Fpn was highly expressed by cells supplemented with iron for 5-7 days (+Fe). At 2h-Fe and 4h-Fe, the expression of Fpn increased but subsequently decreased by 24h-Fe.

A comparison of Fpn expression with total cellular iron content indicates that P19 cells upregulate iron export in response to extracellular iron. When this iron supplement is withdrawn, Fpn expression remains elevated until intracellular iron stores return to baseline values, after approximately 4 hours. Interestingly, when Fpn expression returns to baseline at 24h-Fe, cellular iron content rises sharply despite the absence of an extracellular iron supplement. The +Fe samples indicate active iron import, presumably through TfRc (Figure 1.1); although, the status of TfRc was not examined in the context of this study. In summary, expression of Fpn in P19 cells is influenced by the presence of extracellular iron.

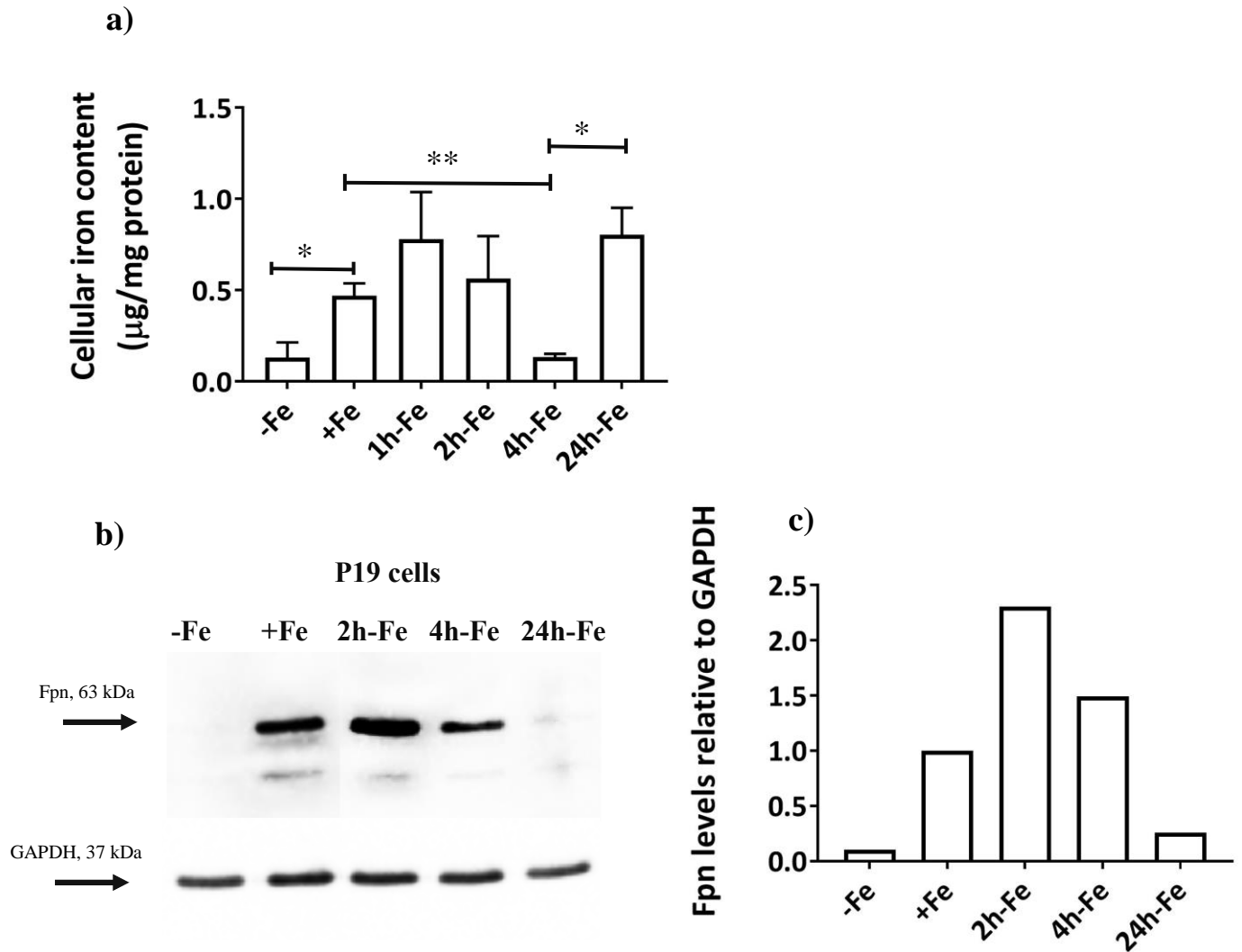


**Figure 2.3. Iron handling in P19 cells under various conditions of extracellular iron supplementation.**

Cells were cultured either in non-supplemented medium (-Fe) or iron-supplemented medium (+Fe) for 5-7 days before iron supplementation withdrawal and an additional 1 (1h-Fe), 2 (2h-Fe), 4 (4h-Fe) or 24 (24h-Fe) hours of culture in non-supplemented medium. **a)** Total cellular iron content was measured by ICP-MS and normalized to total amount of protein. A biphasic pattern was observed in total cellular iron content. -Fe: N=4; +Fe: N=9; 1h-Fe: N=3; 2h-Fe: N=3; 4h-Fe: N=3; 24h-Fe: N=20. Data are the mean  $\pm$  SEM (\*,  $p < 0.05$ ; \*\*,  $p < 0.01$ ; \*\*\*,  $p < 0.001$ ). **b)** Protein lysates from P19 cells were examined by Western blot, probed with anti-ferroportin 1 (top panel) and anti-GAPDH (bottom panel). Approximate M.W. is indicated in the left margin. **c)** The signal intensity

of each Fpn band was normalized to the corresponding GAPDH band. All bars are normalized to the +Fe condition (N=1). Fpn expression increases in response to extracellular iron and decreases within 24 hours of the removal of extracellular iron supplementation.

### 2.3.1.3 MRI Relaxation Rates

To examine possible changes in MR relaxation rates under various conditions of iron supplementation, cells were cultured as described in Figure 2.1, first row, then harvested and scanned at 3T using a spherical gelatin phantom. Figure 2.4a shows the signal intensity map of a representative phantom set up for three different TE values in the  $T_2^*$  weighted image. The corresponding signal decay curve for +Fe and -Fe samples in the phantom (denoted by number 1 and 2, respectively) as well as the  $R_2^*$  map for the phantom are shown in Figure 2.4b and c, respectively. Mean values of transverse relaxation rates are shown in Figure 2.5a-c. Relaxation rate measurements showed the same biphasic pattern as observed with total cellular iron content (Figure 2.3a) over the treatment timeframe. As shown in Figure 2.5a,  $R_2^*$  showed a significant increase after iron supplementation compared to untreated cultures (-Fe vs. +Fe,  $p<0.001$ ), consistent with the avid iron import activity in P19 cells reported in a previous study (12). Upon removal of extracellular iron supplementation,  $R_2^*$  decreased to baseline levels within 4 hours (+Fe vs. 4h -Fe,  $p<0.001$ ), consistent with reported iron export activity in P19 cells (12) and clarifying the time course of iron export. Similar to the biphasic pattern observed in cellular iron content (Figure 2.3a), an increase in  $R_2^*$  was also observed at 24h-Fe (4h-Fe vs. 24h-Fe,  $p=0.070$ ,  $N=9$ ) and approached statistical significance.

As previously described, the total transverse relaxation rate,  $R_2^*$  consists of two components:  $R_2$  and  $R_2'$ . The same comparisons were investigated for each component as well (Figure 2.5 b and c). A biphasic pattern was also observed in  $R_2$  and  $R_2'$  over the treatment timeframe, consistent with iron handling behavior in P19 cells. Statistical differences were examined as follow. For  $R_2$ : -Fe vs. +Fe,  $p<0.001$ ; +Fe vs. 4h-Fe,  $p<0.01$ ; and 4h-Fe vs. 24h-Fe,  $p=0.080$ . For  $R_2'$ , -Fe vs. +Fe,  $p<0.05$ ; +Fe vs. 4h-Fe,  $p<0.05$ ; and 4h-Fe vs. 24h-Fe,  $p=0.058$ .

For all relaxation rates, there was no significant difference between +Fe versus 1h-Fe, but the observed rise one hour after withdrawal of iron supplement is consistent with a high level of cellular iron content as shown in Figure 2.3a.

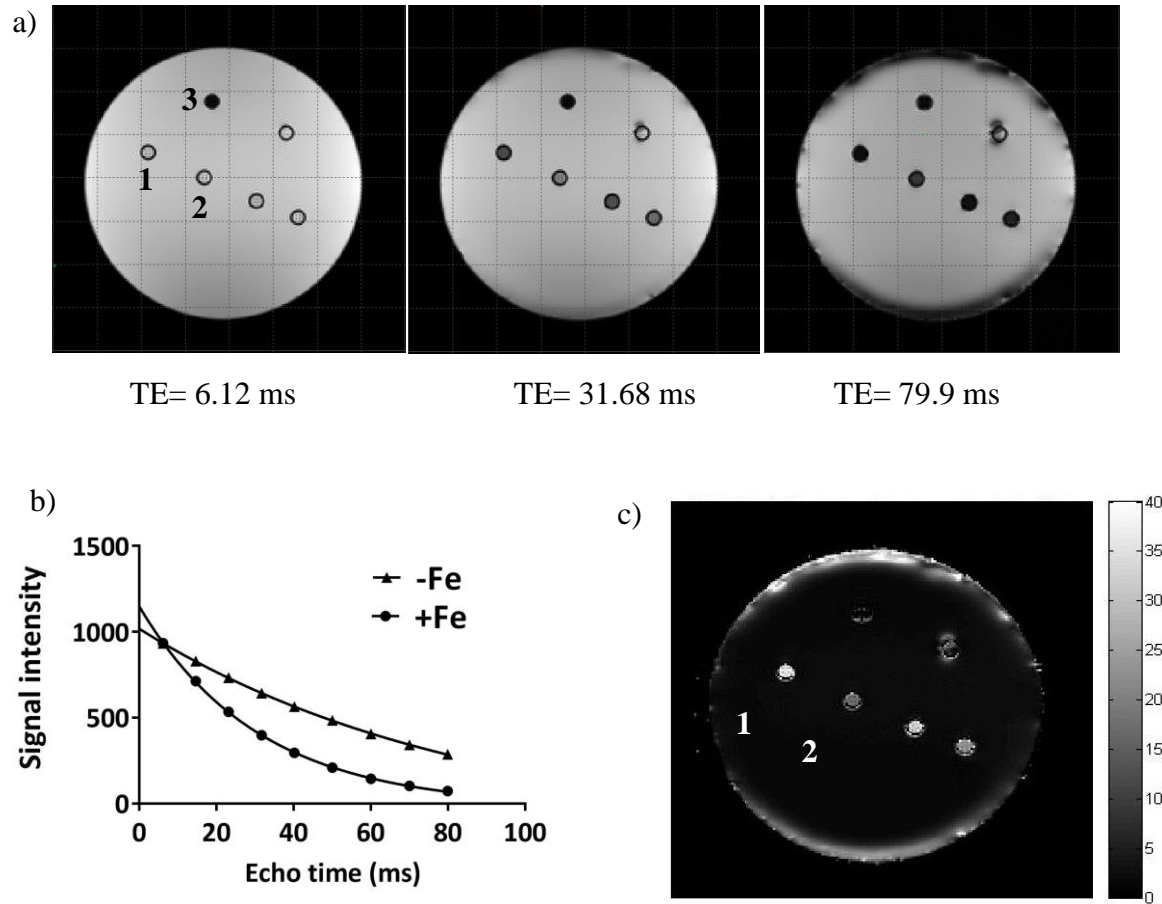


**Figure 2.4. Transverse relaxation rate measurement and mapping in the spherical phantom.**

a) Signal intensity decreases over time in a  $T_2^*$  weighted image for a representative phantom set up. +Fe and -Fe samples are denoted by numbers 1 and 2, respectively. Number 3 shows the plastic peg for reference.

b) Signal decay curves are shown for +Fe and -Fe conditions. Each point shows the mean signal intensity measured within the defined ROI. The best fit for an exponential decay is shown by each curve. Iron supplementation resulted in an increase in  $R_2^*$ .

c) The  $R_2^*$  map illustrates a representative phantom. The map was obtained using voxel by voxel curve fitting with an exponential decay function. Higher  $R_2^*$  is observed for the +Fe condition (1) compared to -Fe (2).

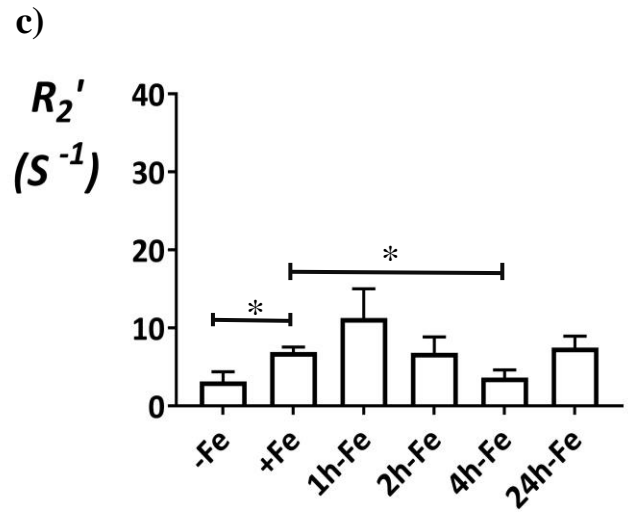
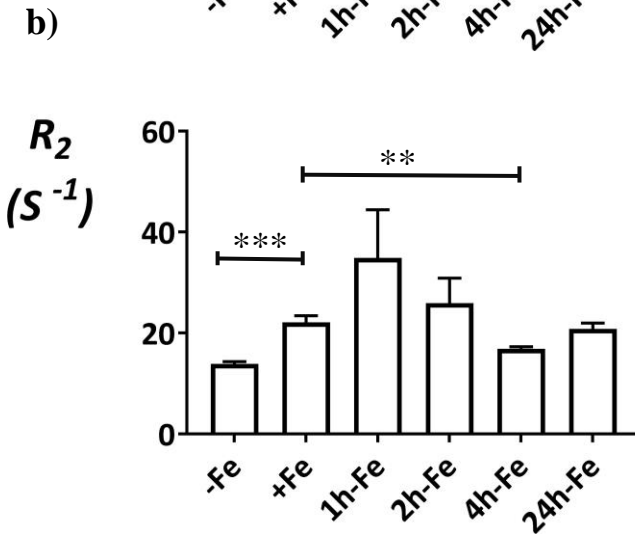
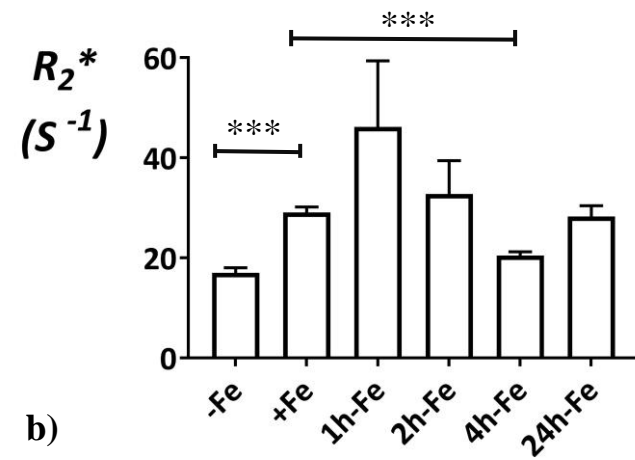


**Figure 2.5. Transverse relaxation rates of P19 cells under various conditions of extracellular iron supplementation.**

Cells were cultured either in non-supplemented medium (-Fe) or iron-supplemented medium (+Fe) for 5-7 days before iron supplementation withdrawal and an additional 1 (1h-Fe), 2 (2h-Fe), 4 (4h-Fe) or 24 (24h-Fe) hours of culture in non-supplemented medium. **a, b)**  $R_2^*$  and  $R_2$  were determined at 3T and **c)**  $R_2'$  was calculated for each sample:  $R_2' = R_2^* - R_2$ . A significant increase in each transverse relaxation rate was observed after iron supplementation, consistent with active iron import in P19 cells. Within 4 hours of the withdrawal of extracellular iron supplement, the signal returned to baseline, consistent with an increase in iron export protein. This finding substantiates dynamic iron regulation in P19 cells. -Fe: N=4; +Fe: N=9; 1h-Fe: N=3; 2h-Fe: N=3; 4h-Fe: N=3; 24h-Fe: N=9. Data are the mean  $\pm$  SEM (\*,  $p < 0.05$ ; \*\*,  $p < 0.01$ ; \*\*\*,  $p < 0.001$ ).



## 2.3.2 P19 Response to Hepcidin Treatment

### 2.3.2.1 Analysis of Intracellular Iron Content

To investigate the effect of hepcidin on the total cellular iron content, two conditions were examined. Cells were cultured in the presence of 25  $\mu$ M ferric nitrate/medium for 5-7 days (+Fe). Then they were incubated with or without 200 ng/ml hepcidin for the last 24 hours of the culture in iron supplemented (+Fe +H) or non-supplemented (24h-Fe +H) medium. The aim was to explore if any further increase in cellular iron content was achievable, beyond the +Fe or 24h-Fe condition, by blocking iron export activity in these cells. As shown in Figure 2.6a, no significant difference was observed in total cellular iron content between hepcidin and non-hepcidin treated cells.

### 2.3.2.2 Expression of Ferroportin

To examine the possibility of hormonal regulation of iron export in P19 cells, cultures were supplemented with iron for 5-7 days (+Fe). Cells were harvested after withdrawal of iron supplement and culture in non-supplemented medium for an additional 2 (2h-Fe), 4 (4h-Fe) and 24 (24h-Fe) in the presence of 200 ng/ml hepcidin. In addition, cells incubated in non-supplemented medium (-Fe) and iron supplemented medium (+Fe) were treated with hepcidin for the last 24 hours of their culture. Western blots were used to detect potential changes in Fpn expression in response to hepcidin treatment and compared to non-hepcidin treated cells. As shown in Figure 2.6b and c versus Figure 2.3b and c, Fpn immunostaining decreased in the presence of hepcidin (2h-Fe and 4h-Fe). Also, densitometric analysis showed that Fpn immunostaining decreased in a continuously iron-supplemented sample (+Fe +H) by approximately %50 after hepcidin treatment. This finding suggests that iron-stimulated expression of Fpn is distinct from hepcidin-mediated degradation of Fpn. As expected, the low level of Fpn expression in -Fe and 24h-Fe samples did not change in the presence of hepcidin.

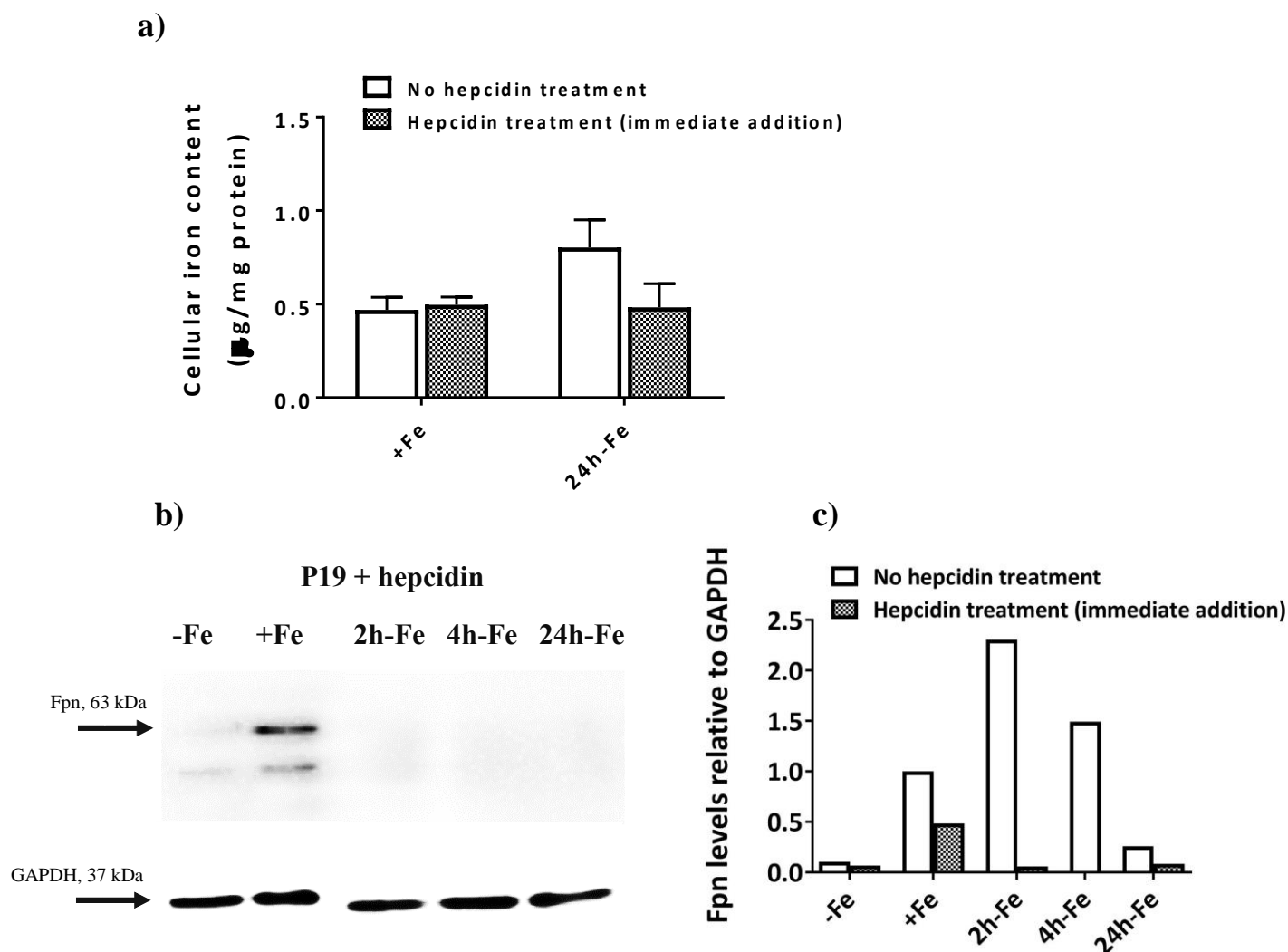


**Figure 2.6. Cellular iron handling in P19 cells in response to hepcidin treatment.**

Cells were cultured either in non-supplemented medium (-Fe) or iron-supplemented medium (+Fe) for 5-7 days before iron supplementation withdrawal and an additional 2 (2h-Fe), 4 (4h-Fe) or 24 (24h-Fe) hours of culture in non-supplemented medium, with or without hepcidin. In the case of hepcidin treatment +/-Fe, cells were incubated with hepcidin for the last 24 hours of culture. **a)** Total cellular iron content for +Fe and 24h-Fe was measured by ICP-MS and normalized to total amount of protein for samples treated with (gray bars) or without (white bars) hepcidin. No significant difference was observed between treatment groups. +Fe (no hepcidin), N=9; +Fe (hepcidin treatment), N=6; 24h-Fe (no hepcidin), N=20; 24h-Fe (hepcidin treatment), N=3. **b)** Proteins lysates of

hepcidin treated cells were examined by Western blot, probing with anti-ferroportin 1 (top panel) and anti-GAPDH (bottom panel). Approximate M.W. is shown in the left margin. **c)** The signal intensity of each Fpn band was normalized to the corresponding GAPDH band. The signal intensity of Fpn at 4h-Fe with hepcidin was below the detection limit. All ratios were subsequently normalized to the +Fe condition. Fpn expression was downregulated in response to hepcidin (N=1).

### 2.3.2.3 MRI Relaxation Rates

As described in section 2.3.2.1, +Fe and 24h-Fe conditions were first chosen to explore the effect of hepcidin on cellular iron content and MR transverse relaxation rates. Cells were incubated in the presence or absence of hepcidin for the last 24 hours of the culture and then scanned at 3T to measure transverse relaxation rates. In Figure 2.7, mean values of a)  $R_2^*$ , b)  $R_2$  and c)  $R_2'$  are shown. No significant difference in transverse relaxation rates were observed between hepcidin and non-hepcidin treated P19 cells.

In addition to the conditions examined above, we investigated the effect of hepcidin on P19 cells using a different treatment timeline (Figure 2.1, second row). Cells were cultured in iron-supplemented medium for 5-7 days before an additional 2 (2h-Fe) or 4 (4h-Fe) hours culture in non-supplemented medium. Instead of immediate addition, hepcidin was added to the medium one hour after iron supplementation withdrawal. As mentioned earlier, P19 cells efficiently export iron within the first hour of iron supplementation withdrawal. By adding hepcidin at 1h-Fe, we aimed to interrupt iron export at a time in which it was actively occurring. Cellular iron content and relaxation rates were compared to those of cells without hepcidin treatment. Comparing mean values showed no statistical significant difference between hepcidin and non-hepcidin treated cells (Figure A, Appendix A).

While Fpn expression was altered, the non-significant difference observed in total cellular iron content and transverse relaxation rates, before and after hepcidin treatment, lead us to examine if the correlation between MR signal and cellular iron content had been influenced by hepcidin treatment. The results of this investigation are reported in the next section.

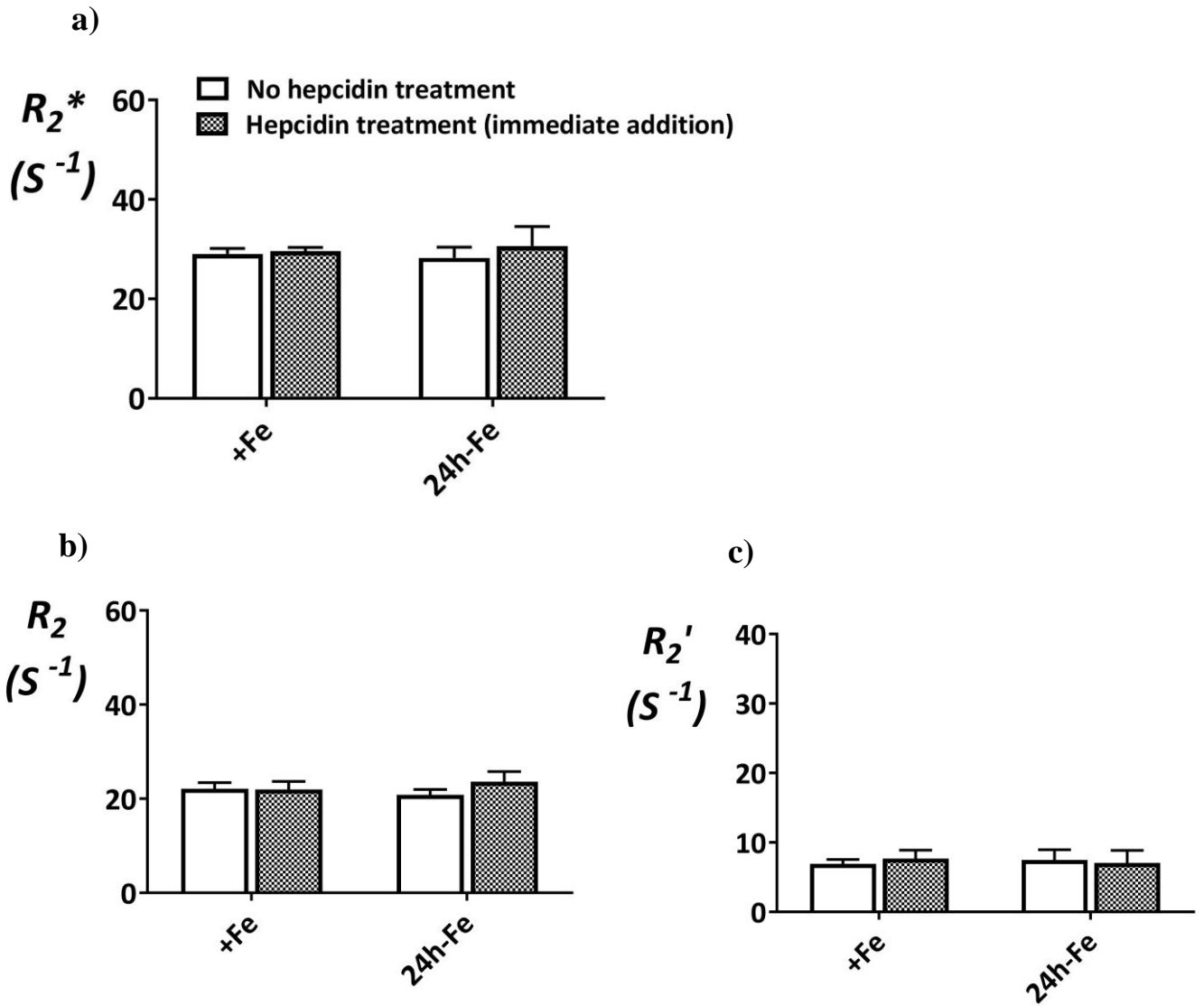


**Figure 2.7. Transverse relaxation rates of P19 cells in response to hepcidin treatment.**

Cells were cultured in iron-supplemented medium (+Fe) for 5-7 days before supplementation withdrawal and an additional 24 (24h-Fe) hours of culture in non-supplemented medium with or without hepcidin. These samples were then compared to cells at +Fe, incubated in the presence and absence of hepcidin for the last 24 hours of their culture. Transverse relaxation rates for **a)**  $R_2^*$  and **b)**  $R_2$  were determined at 3T while  $R_2'$  (**c)** was calculated from the difference:  $R_2' = R_2^* - R_2$ . No significant difference was observed between hepcidin and non-hepcidin treatment groups. +Fe (no hepcidin), N=9; +Fe (hepcidin treatment), N=3; 24h-Fe (no hepcidin), N=9; 24h-Fe (hepcidin treatment), N=8. Data are the mean  $\pm$  SEM.

### 2.3.3 Correlation Between MR Signal and Cellular Iron Content

To understand the correlation between cellular iron and MR signal, samples were separated into their respective treatment groups: hepcidin versus no hepcidin. Pearson's correlation test was applied to investigate any correlation between cellular iron content as the independent variable and transverse relaxation rate as the dependent variable.

In the absence of hepcidin (Figure 2.8 a-c, open circles), there is moderate correlation between  $R_2^*$  and cellular iron content ( $r=0.629$ ,  $p<0.001$ ). A weak correlation between  $R_2$  and cellular iron content ( $r=0.473$ ,  $p<0.01$ ) and a moderate correlation between  $R_2'$  and cellular iron content ( $r=0.749$ ,  $p<0.001$ ) was observed. On the other hand, in the presence of hepcidin (Figure 2.8 a-c, filled circles), a strong correlation was observed between  $R_2^*$  and cellular iron content ( $r=0.851$ ,  $p<0.001$ ) and  $R_2$  and cellular iron content ( $r=0.866$ ,  $p<0.001$ ). However, the correlation between  $R_2'$  and cellular iron content, was weak ( $r=0.532$ ,  $p<0.05$ ; Table 1)

The line of best fit for hepcidin (solid lines) and non-hepcidin (dashed lines) treated cells was determined using a linear regression model (Figure 2.8a-c). The difference between slopes was determined using independent samples t-test. Comparing slopes of the lines for  $R_2^*$  vs. cellular iron (Figure 2.7a) revealed a significant increase from 10.09 for non-hepcidin treated cells to 35.56 for hepcidin treated cells ( $p<0.05$ ). The same analysis for  $R_2$  vs. cellular iron (Figure 2.7b) showed a significant increase in the slope from 5.25 for non-hepcidin treated cells to 27.77 for hepcidin treatment ( $p<0.05$ ). However, for  $R_2'$  vs. cellular iron (Figure 2.7c), no line of best fit was drawn for the hepcidin treatment group due to a non-significant linear correlation ( $p = n.s$ ), while the linear correlation for non-hepcidin treated cells was significant.

Finally, for each treatment group, the strength of these linear correlations was compared using Fisher Z transformation. The analysis showed no significant difference between the relation of elemental iron and  $R_2^*$ , elemental iron and  $R_2$ , and elemental iron and  $R_2'$ . In summary, no single linear correlation was significantly more outstanding compared to the others, in each treatment group.

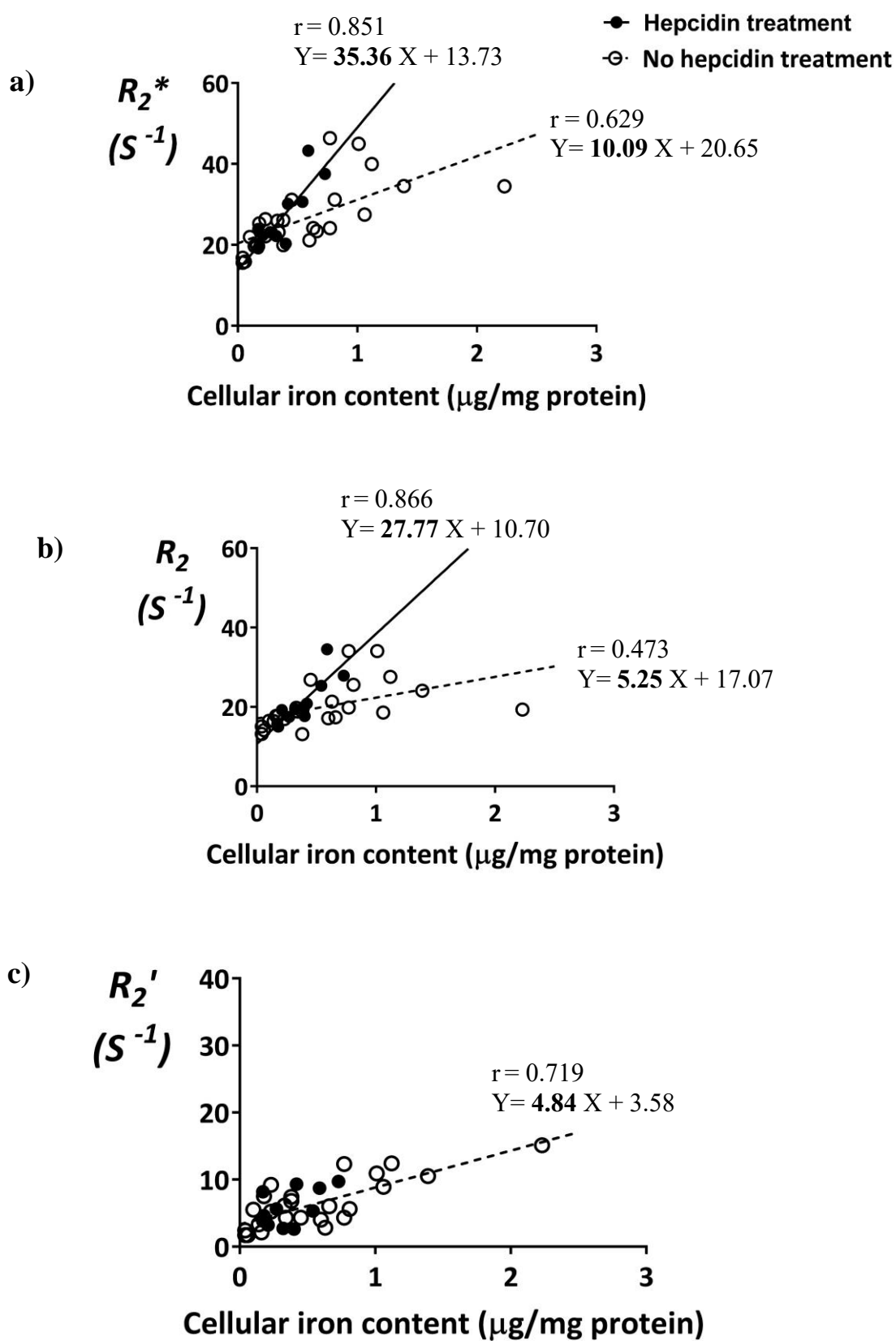


Figure 2.8 Comparison of MR relaxation rates and total cellular iron content in P19

cells.

Cells were cultured in the absence (empty circles, N=25) or presence (filled circles, N=11) of hepcidin under various conditions of extracellular iron supplementation. Total cellular iron content was determined by ICP-MS and normalized to total cellular protein. Transverse relaxation rates were obtained at 3T. Pearson's correlation and regression analysis were applied to investigate the relationship between relaxation rates and cellular iron content. Hepcidin treatment significantly increases slopes of the line relating  $R_2^*$  vs. cellular iron and  $R_2$  vs. cellular iron. However, no significant linear relationship was found between  $R_2'$  vs. cellular iron after hepcidin treatment.

**Table 1. Correlation between MR relaxation rates and total cellular iron content in P19 cells.**

	<sup>a</sup> Whole data (N=36)	No hepcidin treatment (N=25)			Hepcidin treatment (N=11)			Difference between slopes
	<sup>b</sup> r	r	<sup>b</sup> β	r <sup>2</sup>	r	β	r <sup>2</sup>	
$R_2^*$	0.607 p<0.001	0.629 p<0.001	<b>10.09</b>	0.369 p<0.001	0.851 p<0.001	<b>35.36</b>	0.724 p<0.001	<b>p&lt;0.05</b>
$R_2$	0.468 p<0.01	0.473 p<0.01	<b>5.25</b>	0.224 p<0.05	0.866 p<0.001	<b>27.77</b>	0.751 p<0.001	<b>p&lt;0.01</b>
$R_2'$	0.679 p<0.001	0.719 p<0.001	4.84	0.517 p<0.001	0.532 p<0.05	<sup>c</sup> n.s	n.s p=0.92	<sup>c</sup> n/a

<sup>a</sup> Statistical analysis of the whole data set combines samples treated with (N=11) and without (N=25) hepcidin. N: sample size.

<sup>b</sup> r: Pearson correlation coefficient; p: level of significance; β: linear regression slope.

<sup>c</sup> n.s: not significant; n/a: not applicable.



## 2.4 Discussion

In this study, we examined the influence of extracellular iron and the endocrine hormone hepcidin on MRI using multi-potent mouse P19 embryonic teratocarcinoma cells to model the regulation of iron export activity. Hepcidin is a hepatic hormone which is upregulated in response to inflammation. Alterations in MR transverse relaxation rates and cellular iron content as well as expression of the iron export protein, Fpn, were investigated in response to hepcidin, using P19 cells cultured under various conditions of extracellular iron supplementation (Figure 2.1). The results revealed that hepcidin-dependent alterations in iron homeostasis are detectable by MRI. In addition, intracellular iron content and ferroportin were regulated in a biphasic manner in response to changes in extracellular iron.

### **Intracellular iron analysis**

Iron uptake by mammalian cells is mainly through Tf-TfRc interactions in which Tf-bound iron is internalized by receptor-mediated endocytosis. While iron is a vital element for cellular homeostasis, excess iron can cause oxidative damage by creating reactive oxygen species. As a result, the level of iron uptake is balanced by regulation of TfRc protein in most cells. When internalized iron is not immediately used, it is mainly sequestered in the storage protein ferritin, as a biomineral. Finally, in select cells, iron is exported by Fpn, the sole iron export protein in vertebrates (19, 20). In our P19 cell model, total cellular iron content significantly increased in iron-supplemented culture compared to non-supplemented culture (Figure 2.3a), indicating effective iron internalization. This observation in P19 cells is similar to that reported in mouse bone marrow-derived macrophages (5). After removal of iron supplementation from P19 cell culture, total cellular iron content decreased within 4 hours, suggesting high iron export activity. However, a second rise in total cellular iron content in P19 cells occurred 24 hours after withdrawal of iron supplementation (24h-Fe; Figure 2.3a). Fpn expression was minimal at this time point (Figure 2.3b and c), confirming that iron export has been downregulated. While the rise in the total cellular iron content at 24h-Fe should be influenced by iron import activity, our results nevertheless point to the sensitive regulation of iron export protein in response to changes in extracellular iron.

Hepcidin has been reported to trigger internalization and downregulation of Fpn in the reticuloendothelial system (21-24). As a result, iron accumulation has been observed as an increase in ferritin level. In our study, we compared total cellular iron content in P19 cells treated with and without hepcidin, and found no significant change in total cellular iron. This may be explained by the fact that elemental analysis of total cellular iron includes all forms of iron and does not distinguish fluctuations in ferritin or the labile iron pool (LIP). Internalized iron first enters the LIP before being stored in ferritin as Fe (III) or exported by Fpn. Although LIP represents a small fraction of the total cellular iron content under quiescent conditions, this may be dramatically altered in response to biochemical stimuli (25-27). Hepcidin-associated decrease in iron export in P19 cells may influence LIP integrity. One hypothesis is that an increase in ferritin level might be balanced by a decrease in LIP, which ultimately results in a constant level of total cellular iron content. In addition, TfRc expression may be altered in response to an increase in the level of intracellular iron, to maintain cellular iron homeostasis. As mentioned earlier, increases in the level of cellular iron alters IRP/IRE binding, resulting in a decrease in TfRc expression. These hypotheses still need to be investigated in the P19 cell model.

### **Protein Analysis**

Fpn is known to be expressed by a few cell types including macrophages, enterocytes, hepatocytes and breast epithelia (28-30). Macrophages have a principal role in phagocytosis of damaged or senescent red blood cells, exporting microgram quantities of iron back into plasma for the synthesis of new red blood cells. This iron recycling proceeds through a Fpn-mediated pathway. Fpn upregulation in macrophages after iron supplementation and erythrophagocytosis has been shown in several studies (5, 24, 31, 32). A similar pattern was observed in the P19 cell study herein after supplementation with extracellular iron. On the other hand, Fpn downregulation has been reported when macrophages were exposed to desferrioxamine mesylate (DFO) (5, 31). DFO binds iron particles, depriving the cell of iron. Hence, it provides a similar culture condition to what was examined in this study by withdrawal of iron supplementation. We observed a

decrease in Fpn expression within 4 hours and the absence of Fpn by 24 hours. The similar pattern of Fpn expression in P19 cells and macrophages in response to extracellular iron supplementation is an interesting finding and suggests that characteristics of iron homeostasis in P19 cells may be relevant to macrophage function.

In our study, downregulation of Fpn was observed 24 hours after removal of iron supplementation, when no hepcidin treatment was administered. The expression of Fpn stimulated by extracellular iron (+Fe) and its turnover after removal of iron supplementation (at 24h-Fe) suggests that post-translational regulation of Fpn may be active. There are two known mechanisms for post-translational regulation of Fpn. Its downregulation in the absence of multicopper oxidases has been reported (33). This does not likely explain our results since no treatment related to multicopper oxidases was performed. The second known mechanism is hepcidin-dependent downregulation of Fpn, which raises the possibility of hepcidin production by P19 cells to self-regulate Fpn expression post-translationally. Further investigation is warranted.

In inflammation, Fpn is post-translationally downregulated in macrophages by the hormone hepcidin (19, 34), which itself is upregulated by inflammation and serum iron level (6, 35, 36). Hepcidin-dependent internalization and downregulation of Fpn have been shown in HEK293 cells expressing mouse Fpn (22, 23, 37), mouse primary bone marrow-derived macrophages (22, 32) and the mouse macrophage cell line J774 (24). Our results confirmed downregulation of Fpn in P19 cells in response to hepcidin (Figure 2.6b and c) suggesting that this cell line may be a suitable model for further investigation of hepcidin-dependent Fpn regulation.

As discussed earlier, anti-inflammatory (M2) macrophages exhibit high expression of Fpn, resulting in an iron recycling phenotype. This pattern of iron export is also displayed by tumor-associated macrophages (TAM) (38) and provides a ready supply of iron for uncontrolled tumour growth. On the other hand, pro-inflammatory (M1) macrophages express Fpn at a minimal level and represent an iron storage phenotype (5, 29). In this context, the parental P19 cell line shows similar iron handling activities and Fpn expression as M2 macrophages and TAM. Interestingly, P19 are also a rapidly growing

cell type, doubling in less than 24 hours. This characteristic may be facilitated by their iron recycling ability. In addition, hepcidin-mediated degradation of Fpn indicates that P19 cells are capable of responding to pro-inflammatory signalling and converting to select features of M1 macrophages. This may provide an opportunity to study macrophage-related iron handling behaviour using an easy to culture cell line: P19.

### **MRI analysis**

MRI is a promising tool for molecular imaging. Paramagnetic compounds, such as iron-based contrast agents, shorten longitudinal and transverse relaxation times (and hence increase relaxation rates) in the tissues where they accumulate. This results in a brightening of  $T_1$ -weighted images and a darkening of  $T_2$ -weighted images (39). In any case, the way cells handle iron in these tissues is expected to affect the MR signal. In particular, since macrophages have distinct iron handling mechanisms, it may be possible to distinguish the M1 pro-inflammatory phenotype from the M2 anti-inflammatory phenotype using MRI. M1 macrophages express low Fpn and high ferritin and hence show iron storage properties, while M2 macrophages express high Fpn and low ferritin, representing an iron recycling phenotype. Low Fpn expression in M1 macrophages is partially associated with systemic hepcidin upregulation, as a result of iron overloading or inflammation. Once we established that P19 cells are a good model to study macrophage-like iron homeostasis, we investigated the effect of iron supplementation and hepcidin on MR transverse relaxation rates.

In response to changes in extracellular iron, transverse relaxation rate measurements in P19 cells showed the same biphasic pattern as observed in total cellular iron content over the treatment timeframe (Figure 2.5). In all three transverse relaxation rates, a significant increase was observed after culture in iron supplementation. This was followed by a significant decrease in relaxation rates within 4 hours of iron withdrawal. Similar to cellular iron measurements, a second increase was observed in transverse relaxation rates by 24 hours post-iron withdrawal ( $p=0.070$ ). This result suggests that MRI faithfully tracks changes in cellular iron content, particularly when regulation of iron export is involved.

To compare the results of the current and a previous study in our lab (12), it is worthwhile to first mention the similarities and differences in the experimental conditions. Although the same cell line was used in both studies and they were supplemented with extracellular iron for the same duration (5-7 days), the concentration of ferric nitrate in the iron supplemented medium was different. In the present study, 25  $\mu\text{M}$  ferric nitrate was used, whereas in Liu's study, medium was supplemented with 250  $\mu\text{M}$  ferric nitrate. The increase observed in transverse relaxation rates in P19 cells after iron supplementation was similar to Liu's study. However, in the present report, all three transverse relaxation rates showed a significant increase in magnitude at 24h-Fe (compared to the baseline) while in Liu's work these parameters returned to baseline values at 24h-Fe. This might be explained by the different conditions of iron supplementation.

Influence of hepcidin on MR transverse relaxation rates was examined in P19 cells. This was done to mimic the hepcidin-dependent alteration in macrophage iron homeostasis using our cell model and to investigate its effect on MR detection. No significant changes in any of the transverse relaxation rates were observed (Figure 2.7) by virtue of hepcidin-mediated Fpn degradation. While this finding was consistent with total cellular iron content measured in P19 samples, we examined if downregulation of Fpn might alter other aspects of intracellular iron handling not reflected by the magnitude of the MR signal.

The correlation between total cellular iron content and each transverse relaxation rate was examined for hepcidin treated and non-hepcidin treated groups (Figure 2.8). In the absence of hepcidin, a significant moderate correlation was observed between iron and  $R_2^*$  as well as  $R_2'$  ( $r = 0.629$  and  $0.719$ , respectively); however, a weak correlation was observed between iron and  $R_2$  ( $r = 0.473$ ). For hepcidin treated samples, however, the correlation between total cellular iron content and transverse relaxation rates was surprising. Although no significant difference was observed in the magnitude of transverse relaxation rates between hepcidin and non-hepcidin treated groups, the correlation between each relaxation rate and total cellular iron content was significantly different between the two groups. A strong correlation was observed between total

cellular iron content and  $R_2^*$  as well as  $R_2$  in the hepcidin treated group ( $r = 0.851$  and  $0.866$ , respectively). However, no significant correlation was observed between total cellular iron content and  $R_2'$ , suggesting that hepcidin treatment decreases the influence of this reversible component on the total transverse relaxation rate,  $R_2^*$ . In addition, when the slopes of the best fit lines were compared between the two groups, these were significantly higher in hepcidin treated groups compared to non-hepcidin groups (Table 1).

Since total cellular iron content did not significantly change upon hepcidin treatment, other factor(s) may underlie these changes in the correlation between iron and relaxation rate. One hypothesis is that Fpn degradation by hepcidin results in a re-arrangement of total cellular iron. For example, cellular iron is mainly available in two forms: as an iron oxide bound to ferritin, consisting of ferric ion (Fe III), and as unbound iron in the labile iron pool, in the ferrous form (Fe II). The chemical state of iron (ferrous versus ferric) and its compartmentalization (free versus protein bound) are two main factors that change when intracellular iron is redistributed. As a result, spin-spin interactions between iron particles and adjacent atoms may be affected and alter the contribution of reversible and irreversible components to the total transverse relaxation rate. Follow-up experiments should investigate possible changes in LIP and ferritin level resulting from hepcidin-dependent degradation of Fpn in P19 cells.

Iron particles shorten  $T_1$  and  $T_2$ , resulting in a signal increase in  $T_1$  weighted images (positive contrast) while producing a signal loss in  $T_2$  weighted images (negative contrast). We only examined  $T_2$  weighted images and compared transverse relaxation rates since prior results in P19 cells showed that longitudinal relaxation rate did not reflect cellular iron content when supplementing cultures with extracellular iron (12). However, if hepcidin activity alters the LIP as proposed above, that might also influence  $T_1$  since it depends on the energy transfer between spins and the lattice. Thus, if the chemical form of surrounding atoms or their compartmentalization is altered under different conditions of iron supplementation and hepcidin-mediated regulation of iron export, this might influence the efficiency of energy transfer and therefore,  $T_1$ .

**Conclusion:**

Iron handling mechanisms in different cell types may influence cell tracking with MRI. This may apply particularly to the tracking of macrophages, as important components of inflammation signaling show distinct iron handling activities. Using P19 cells, a potential model for M2 anti-inflammatory macrophages, we examined the effect of different conditions of iron supplementation on Fpn expression, total cellular iron content and the MR signal. In addition, the possible effect of hepcidin on Fpn expression, cellular iron content and the MR signal was investigated in P19 cells, to examine the potential for modeling M1 pro-inflammatory macrophage iron handling behavior.

A significant increase in total cellular iron content after supplementation with extracellular iron, followed by a significant decrease after removal of iron supplementation, confirmed the iron import and export abilities of P19 cells. This observation was matched to fluctuations in the pattern of Fpn iron export protein expression. Hepcidin treatment resulted in Fpn degradation in P19 cells, consistent with the reported activity of hepcidin (23). Altogether, P19 cells showed the potential to model macrophage iron-handling activity. Importantly, this phenomenon was associated with a significant change in the way P19 MR signals correlated with total cellular iron content. In hepcidin-treated cells, a strong correlation between each transverse relaxation rate and total cellular iron content was observed with a significantly higher slope of the best fit line, compared to non-treated cells. This demonstrates how cellular iron and, more importantly, hepcidin-dependent alteration of iron export might influence the MR signal. Finally, this study indicates the potential for (1) non-invasively distinguishing different macrophage phenotypes based on the control of iron export and (2) monitoring such inflammation-related changes using MRI.

## References

1. Ahmed A.U. *An overview of inflammation: mechanism and consequences*. Frontiers in Biology. 2011;**6**:274-81.
2. Gordon S. *Alternative activation of macrophages*. Nat Rev Immunol. 2003;**3**(1):23-35.
3. Gordon S., Taylor P.R. *Monocyte and macrophage heterogeneity*. Nat Rev Immunol. 2005;**5**(12):953-64.
4. Donovan A., Lima C.A., Pinkus J.L., Pinkus G.S., Zon L.I., Robine S., Andrews N.C. *The iron exporter ferroportin/Slc40a1 is essential for iron homeostasis*. Cell Metab. 2005;**1**:191-200.
5. Corna G., Campana L., Pignatti E., Castiglioni A., Tagliafico E., Bosurgi L., Campanella A., Brunelli S., Manfredi A.A., Apostoli P., Silvestri L., Camaschella C., Rovere-Querini P. *Polarization dictates iron handling by inflammatory and alternatively activated macrophages*. Haematologica. 2010;**95**:1814-22.
6. Sangkhav V., Nemeth E. *Regulation of the Iron Homeostatic Hormone Hepcidin*. Adv Nutr. 2017;**8**(1):126-36.
7. Theurl I., Theurl M., Seifert M., Mair S., Nairz M., Rumpold H., Zoller H., Bellmann-Weiler R., Niederegger H., Talasz H., Weiss G. *Autocrine formation of hepcidin induces iron retention in human monocytes*. Blood. 2008;**111**:2392-9.
8. Ganz T., Nemeth E. *Hepcidin and iron homeostasis*. Biochimica et biophysica acta. 2012;**1823**:1434-43.
9. Li L., Jiang W., Luo K., Song H., Lan F., Wu Y., Gu Z. *Superparamagnetic iron oxide nanoparticles as MRI contrast agents for non-invasive stem cell labeling and tracking*. Theranostics. 2013;**3**:595-615.
10. Goldhawk D.E., Rohani R., Sengupta A., Gelman N., Prato F.S. *Using the magnetosome to model effective gene-based contrast for magnetic resonance imaging*. Wiley Interdiscip Rev Nanomed Nanobiotechnol. 2012;**4**:378-88.
11. Goldhawk D.E., Gelman N., Sengupta A., Prato F.S. *The interface between iron metabolism and gene-based iron contrast for MRI*. Magnetic Resonance Insights. 2015;**8**:9-14.
12. Liu L. Characterization of MagA expression and Iron uptake in P19 cells: Implications for use as a gene-based contrast agent for MRI: Western Univeristy; 2015.



13. Smith P.K., Krohn R.I., Hermanson G.T., Mallia A.K., Gartner F.H., Provenzano M.D., Fujimoto E.K., Goeke N.M., Olson B.J., Klenk D.C. *Measurement of protein using bicinchoninic acid*. Anal Biochem. 1985;**150**(1):76-85.
14. Towbin H., Staehelin T., Gordon J. *Electrophoretic transfer of proteins from polyacrylamide gels to nitrocellulose sheets: procedure and some applications*. Proceedings of the National Academy of Sciences of the United States of America. 1979;**76**(9):4350-4.
15. Thomas C., Oates P.S. *Ferroportin/IREG-1/MTP-1/SLC40A1 modulates the uptake of iron at the apical membrane of enterocytes*. Gut. 2004;**53**(1):44-9.
16. Guida C., Altamura S., Klein F.A., Galy B., Boutros M., Ulmer A.J., Hentze M.W., Muckenthaler M.U. *A novel inflammatory pathway mediating rapid hepcidin-independent hypoferremia*. Blood. 2015;**125**(14):2265-75.
17. Nie X., Li C., Hu S., Xue F., Kang Y.J., Zhang W. *An appropriate loading control for western blot analysis in animal models of myocardial ischemic infarction*. Biochemistry and Biophysics Reports. 2017;**12**:108-13.
18. Sengupta A., Quiaoit K., Thompson R.T., Prato F.S., Gelman N., Goldhawk D.E. *Biophysical features of MagA expression in mammalian cells: implications for MRI contrast*. Frontiers in Microbiology. [Original Research]. 2014;**5**:29.
19. Hentze M.W., Muckenthaler M.U., Galy B., Camaschella C. *Two to tango: regulation of Mammalian iron metabolism*. Cell. 2010;**142**(1):24-38.
20. Pantopoulos K., Porwal S.K., Tartakoff A., Devireddy L. *Mechanisms of mammalian iron homeostasis*. Biochemistry. 2012;**51**(29):5705-24.
21. De Domenico I., Ward D.M., Langelier C., Vaughn M.B., Nemeth E., Sundquist W.I., Ganz T., Musci G., Kaplan J. *The molecular mechanism of hepcidin-mediated ferroportin down-regulation*. Molecular Biology of the Cell. 2007;**18**:2569-78.
22. Qiao B., Sugianto P., Fung E., del-Castillo-Rueda A., Moran-Jimenez M.-J., Ganz T., Nemeth E. *Hepcidin-induced endocytosis of ferroportin is dependent on ferroportin ubiquitination*. Cell Metabolism. 2012;**15**(6):918-24.
23. Nemeth E., Tuttle M.S., Powelson J., Vaughn M.B., Donovan A., Ward D.M., Ganz T., Kaplan J. *Hepcidin regulates cellular iron efflux by binding to ferroportin and inducing its internalization*. Science (New York, NY). 2004;**306**:2090-3.
24. Knutson M.D., Oukka M., Koss L.M., Aydemir F., Wessling-Resnick M. *Iron release from macrophages after erythrophagocytosis is up-regulated by ferroportin 1 overexpression and down-regulated by hepcidin*. Proceedings of the National Academy of Sciences of the United States of America. 2005;**102**(5):1324-8.

25. Kakhlon O., Cabantchik Z.I. *The labile iron pool: characterization, measurement, and participation in cellular processes(1)*. Free Radic Biol Med. 2002;**33**(8):1037-46.
26. Glickstein H., El R.B., Shvartsman M., Cabantchik Z.I. *Intracellular labile iron pools as direct targets of iron chelators: a fluorescence study of chelator action in living cells*. Blood. 2005;**106**(9):3242-50.
27. Pan X., Tamilselvam B., Hansen E.J., Daefler S. *Modulation of iron homeostasis in macrophages by bacterial intracellular pathogens*. BMC Microbiology. 2010;**10**:64-.
28. Abboud S., Haile D.J. *A novel mammalian iron-regulated protein involved in intracellular iron metabolism*. J Biol Chem. 2000;**275**(26):19906-12.
29. Recalcati S., Locati M., Cairo G. *Systemic and cellular consequences of macrophage control of iron metabolism*. Semin Immunol. 2012;**24**(6):393-8.
30. Pinnix Z.K., Miller L.D., Wang W., D'Agostino R., Jr., Kute T., Willingham M.C., Hatcher H., Tesfay L., Sui G., Di X., Torti S.V., Torti F.M. *Ferroportin and iron regulation in breast cancer progression and prognosis*. Sci Transl Med. 2010;**2**(43):3001127.
31. Knutson M.D., Vafa M.R., Haile D.J., Wessling-Resnick M. *Iron loading and erythrophagocytosis increase ferroportin 1 (FPN1) expression in J774 macrophages*. Blood. 2003;**102**(12):4191-7.
32. Delaby C., Pilard N., Gonçalves A.S., Beaumont C., Canonne-Hergaux F. *Presence of the iron exporter ferroportin at the plasma membrane of macrophages is enhanced by iron loading and down-regulated by hepcidin*. Blood. 2005;**106**(12):3979-84.
33. Ward D.M., Kaplan J. *Ferroportin-mediated iron transport: expression and regulation*. Biochim Biophys Acta. 2012;**1823**(9):1426-33.
34. Ganz T., Nemeth E. *Iron homeostasis in host defence and inflammation*. Nat Rev Immunol. 2015;**15**(8):500-10.
35. Schmidt P.J. *Regulation of Iron Metabolism by Hepcidin under Conditions of Inflammation*. The Journal of Biological Chemistry. 2015;**290**(31):18975-83.
36. Camaschella C., Pagani A. *Iron and erythropoiesis: a dual relationship*. Int J Hematol. 2011;**93**(1):21-6.
37. De Domenico I., Lo E., Ward D.M., Kaplan J. *Hepcidin-induced internalization of ferroportin requires binding and cooperative interaction with Jak2*. Proceedings of the National Academy of Sciences of the United States of America. 2009;**106**(10):3800-5.

38. Sica A., Schioppa T., Mantovani A., Allavena P. *Tumour-associated macrophages are a distinct M2 polarised population promoting tumour progression: potential targets of anti-cancer therapy*. Eur J Cancer. 2006;**42**(6):717-27.
39. Hashemi R.H., Bradley W.G., Lisanti C.J. MRI: The Basics, 2nd Edition: Lippincott Williams & Wilkins; 2004.

### 3.1 Summary

In this study, iron regulation in P19 cells and its influence on MR contrast were examined. We found similar iron export activity and regulation in P19 cells as seen in macrophages. The profile of Fpn expression under different conditions of iron supplementation suggested that P19 cells may serve as a potential model of M2 macrophage iron recycling. Moreover, the downregulation of Fpn and iron export in response to hepcidin suggested that P19 cells may mimic M1 macrophage pro-inflammatory signaling. Finally, we showed that MR transverse relaxation rates correlate with total cellular iron content and that hepcidin, a hormone which is secreted in response to inflammation, alters this correlation. These findings may provide a pathway to further developments in monitoring inflammation by MRI.

### 3.2 Future Work

P19 cells showed considerable iron import and export abilities based on measurement of total cellular iron content and transverse relaxation, consistent with a previous study (1). However, a biphasic pattern was observed in these iron measures and in the expression of iron export protein, over the course of extracellular iron supplementation and its subsequent withdrawal from P19 cell culture. This interesting new finding in P19 iron handling should be further characterized by examining how expression of iron import protein, TfRc, contributes to the biphasic pattern.

Little is known about the possibility of hepcidin-independent degradation of Fpn. The only known mechanism proposed for hepcidin-independent degradation of Fpn is related to changes in cellular multicopper oxidase status. Currently, hepcidin-dependent degradation of Fpn is recognized as the main form of post-translational regulation (2,3).

Hence, one hypothesis regarding Fpn degradation after removal of iron supplementation entails the expression of hepcidin by P19 cells. This type of activity has been reported in monocytes (4) and would be consistent with other macrophage-related activity reported in this thesis.

Although hepcidin caused degradation of Fpn in P19 cells, total cellular iron content did not change significantly. This result cannot be compared with previous studies in macrophages (3,5,6) in which changes in ferritin have been mainly monitored. By considering that some portion of cellular iron is available in the transient labile iron pool, one hypothesis is that the expected increase in ferritin is diminished by a decrease in LIP, resulting in an unchanged level of total cellular iron content. Quantification of the P19 LIP in the presence and absence of hepcidin may provide additional insight. Since the chemical state as well as iron compartmentalization differs between ferritin and the LIP, understanding how iron is shuttled between them in response to hepcidin might help us to explain the observed change in the correlation between cellular iron content and MR transverse relaxation rates.

Monocytes, as the precursors of macrophages, have also been investigated in terms of iron handling activities (4). Findings from the current study, about the influence of hepcidin-dependent iron regulation on the MR signal, suggest that a similar effect may potentially be observed when monitoring monocytes. Therefore, it may be worthwhile examining how hepcidin-mediated iron export in monocytes influences MR imaging. The human leukemia THP-1 cell line, which has the capability of differentiating to macrophages, may be used to model monocyte behavior (7).

Magnetosome nanoparticles are iron biominerals found in a membrane-enclosed compartment produced by magnetotactic bacteria in a protein-directed process (8, 9). Single gene expression systems from magnetotactic bacteria, like *magA*, have been used to demonstrate that rudimentary magnetosome-like nanoparticles may be produced in mammalian cells to enhance MR contrast (10, 11). Since iron handling mechanisms vary among different cell types and these may influence the MRI signal, as observed in P19

cells, it will be interesting to investigate how hepcidin and iron export influence iron accumulation and/or compartmentalization in *magA*-expressing cells.

## References

1. Liu L. Characterization of MagA expression and Iron uptake in P19 cells: Implications for use as a gene-based contrast agent for MRI: Western Univeristy; 2015.
2. Ward D.M., Kaplan J. *Ferroportin-mediated iron transport: expression and regulation*. Biochim Biophys Acta. 2012;**1823**(9):1426-33.
3. Nemeth E., Tuttle M.S., Powelson J., Vaughn M.B., Donovan A., Ward D.M., Ganz T., Kaplan J. *Hepcidin regulates cellular iron efflux by binding to ferroportin and inducing its internalization*. Science (New York, NY). 2004;**306**:2090-3.
4. Theurl I., Theurl M., Seifert M., Mair S., Nairz M., Rumpold H., Zoller H., Bellmann-Weiler R., Niederegger H., Talasz H., Weiss G. *Autocrine formation of hepcidin induces iron retention in human monocytes*. Blood. 2008;**111**:2392-9.
5. De Domenico I., Ward D.M., Langelier C., Vaughn M.B., Nemeth E., Sundquist W.I., Ganz T., Musci G., Kaplan J. *The molecular mechanism of hepcidin-mediated ferroportin down-regulation*. Molecular Biology of the Cell. 2007;**18**:2569-78.
6. Qiao B., Sugianto P., Fung E., del-Castillo-Rueda A., Moran-Jimenez M.-J., Ganz T., Nemeth E. *Hepcidin-induced endocytosis of ferroportin is dependent on ferroportin ubiquitination*. Cell Metabolism. 2012;**15**(6):918-24.
7. Bosshart H., Heinzelmann M. *THP-1 cells as a model for human monocytes*. Annals of Translational Medicine. 2016;**4**(21):438.
8. Komeili A. *Molecular mechanisms of compartmentalization and biomineralization in magnetotactic bacteria*. FEMS microbiology reviews. 2012;**36**:232-55.
9. Uebe R., Schuler D. *Magnetosome biogenesis in magnetotactic bacteria*. Nat Rev Microbiol. 2016;**14**(10):621-37.
10. Goldhawk D.E., Gelman N.R., Thompson T., Prato F.S. Forming Magnetosome-like Nanoparticles in Mammalian Cells for Molecular MRI In *Design and Applications of Nanoparticles in Biomedical Imaging* (Bulte, J, and Modo, M, Eds). Switzerland: Springer International Publishing; 2017. p. 187-203.
11. Goldhawk D.E., Rohani R., Sengupta A., Gelman N., Prato F.S. *Using the magnetosome to model effective gene-based contrast for magnetic resonance imaging*. Wiley Interdiscip Rev Nanomed Nanobiotechnol. 2012;**4**:378-88.

## Appendices

## Appendix A: P19 response to hepcidin treatment (hepcidin added at 1h-Fe).

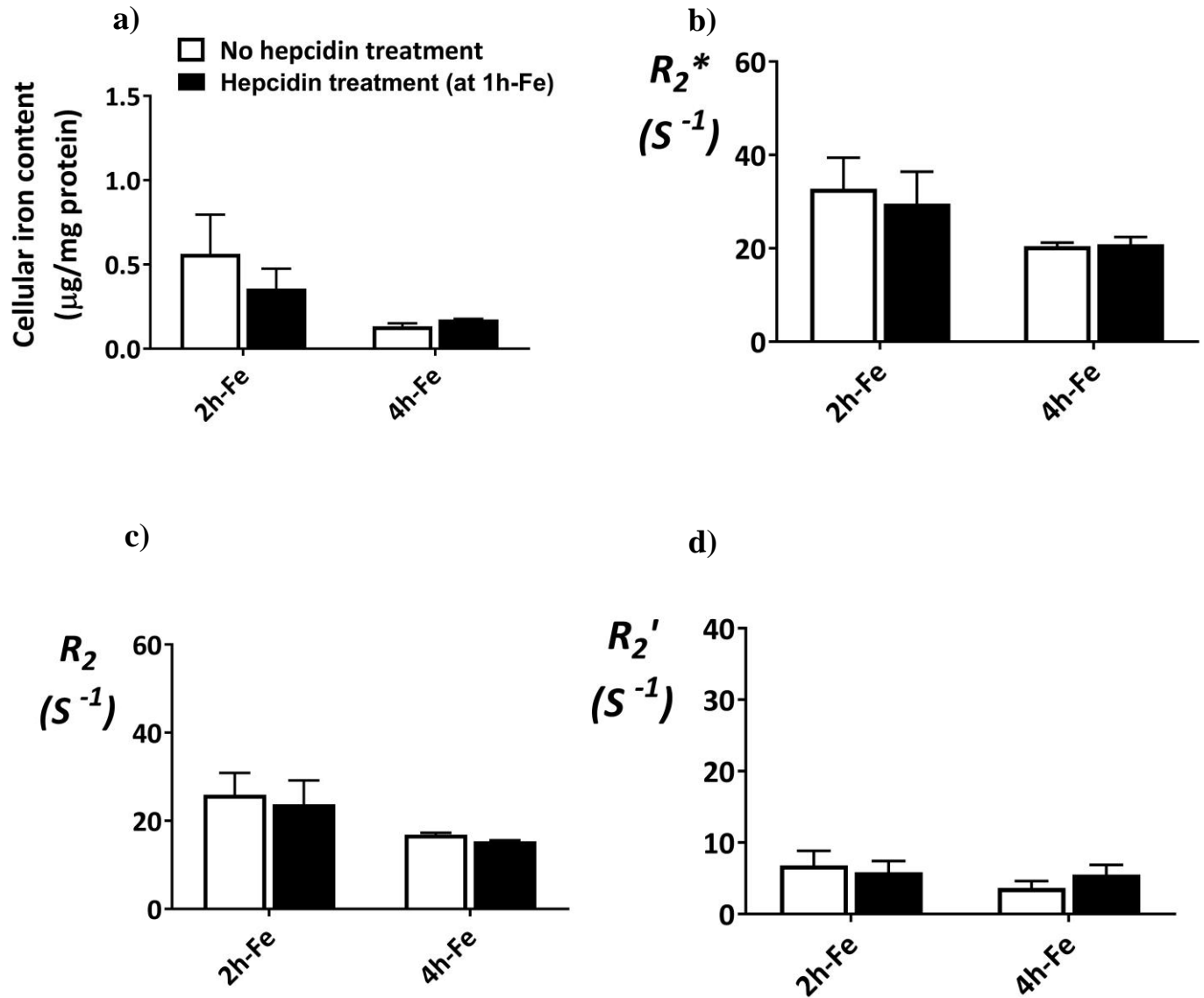


**Figure A. P19 response to hepcidin treatment.** Cells were cultured in iron-supplemented medium (+Fe) for 5-7 days before supplementation withdrawal and an additional 2 (2h-Fe) or 4 (4h-Fe) hours of culture in non-supplemented medium with or without hepcidin addition at 1h-Fe. **a)** Total cellular iron content was measured by ICP-MS and normalized to total amount of protein. 2h-Fe (no hepcidin): N=3; 2h-Fe

(hepcidin treatment): N=3; 4h-Fe (no hepcidin): N=3; 4h-Fe (hepcidin treatment): N=3. **b, c)**  $R_2^*$  and  $R_2$  were determined at 3T and **d)**  $R_2'$  was calculated for each sample:  $R_2' = R_2^* - R_2$ . No significant difference was observed between hepcidin and non-hepcidin treated groups. 2h-Fe (no hepcidin): N=3; 2h-Fe (hepcidin treatment): N=3; 4h-Fe (no hepcidin): N=3; 4h-Fe (hepcidin treatment): N=3. Data are the mean  $\pm$  SEM.



## Curriculum Vitae

<b>Name:</b>	Kobra Alizadeh Pourbouyeh
<b>Post-secondary Education and Degrees:</b>	<p>M.Sc Candidate, Medical Biophysics Western University, London, ON 2016-present.</p> <p>M.Sc, Medical Physics Isfahan University of Medical Sciences, Isfahan, Iran 2011-2014</p> <p>B.Sc, Physics Amirkabir University of Technology, Tehran, Iran 2006-2010</p>
<b>Honours and Awards:</b>	<p>Internal Research Fund (IRF) Lawson Health Research Institute, London, ON 2016-2017</p> <p>Student Travel Stipend World Molecular Imaging Congress, Philadelphia, PA September 2017</p> <p>Travel Award, Institute Community Support Canadian Institutes of Health Research (CIHR), Canada October 2016</p>
<b>Related Work Experience</b>	<p>Physics Teacher Samin High School, Shahriar, Iran 2014-2015</p> <p>Research Assistant Isfahan University of Medical Sciences, Isfahan, Iran 2011-2014</p>

### Publications:

#### Abstract Posters:

- **Alizadeh et al.** Regulation of Iron Export by Heparin is Detectable by Magnetic Resonance Imaging (MRI). World Molecular Imaging Congress (WMIC), Philadelphia, Pennsylvania, USA, September 2017.

- **Alizadeh et al.** The Role of Hepcidin in Monitoring Inflammation by Magnetic Resonance Imaging. World Molecular Imaging Congress (WMIC), Philadelphia, Pennsylvania, USA, September 2017.
- **Alizadeh et al.** Transverse Relaxation Rate in Magnetic Resonance Imaging Is Altered by Hepcidin. Imaging Network Ontario (ImNO), London, Ontario, March 2017.
- **Alizadeh et al.** Hepcidin Activity Provides a Tool to Monitor Inflammation by MRI. Imaging Applications in Prostate Cancer Workshop. London, Ontario, Canada, November 2016.
- **Alizadeh et al.** Influence of Hepcidin on Magnetic Resonance Contrast in P19 Cells. World Molecular Imaging Congress (WMIC), New York City, New York, USA, September 2016.
- **Alizadeh et al.** MagA-derived MR Contrast Persists Despite Cellular Differences in Iron Metabolism. Imaging Network Ontario (ImNO), Toronto, Ontario, March 2016.
- **Alizadeh, K;** Shokrani, P. Estimation of Cardiac and Pulmonary Diseases Probabilities after Breast Cancer Radiotherapy Using Radiobiological Modelling. 11th Iranian Conference of Medical Physics, University of Tehran, Tehran, Iran, 2014.